Lawrence Berkeley Laboratory
UNIVERSITY OF CALIFORNIA

ENERGY & ENVIRONMENT
DIVISION

MULTIPHASE REACTOR MODELING FOR ZINC CHLORIDE CATALYZED COAL LIQUEFACTION

Peter James Joyce
(M.S. thesis)

April 1980

Prepared for the U.S. Department of Energy under Contract W-7405-ENG-48

DISCLAIMER

LBL-9870

Lawrence Berkeley Laboratory
UNIVERSITY OF CALIFORNIA

ENERGY & ENVIRONMENT
DIVISION

MULTIPHASE REACTOR MODELING FOR ZING CHLORIDE CATALYZED COAL LIQUEFACTION

Peter James Joyce
(M.S. thesis)

April 1980

LBL-9870

Multiphase Reactor Modeling for Zinc Chloride Catalyzed Coal Liquefaction

Peter James Joyce

Energy and Environment
Lawrence Berkeley Laboratory
and Department of Chemical Engineering
University of California
Berkeley, California 94720

TABLE OF CONTENTS

LIST OF TABLES

LIST OF FIGURES

To

Peter A. Cahill and Richard T. Kelleher

whose friendship is limitless

ACKNOWLEDGMENT

I would like to take this opportunity to thank those people whose contributions were invaluable with respect to my graduate program.

Professor Ralph A. Troupe of Northeastern University helped me in my preparation for Berkeley.

Professor Henry P. Sheng, John Owyang, and Randy Fishback provided insight and perspective which were extremely helpful with respect to problems encountered at the start of the research.

Stephen Kellner, Tibor Derencsenyi, and Frank Hershkowitz are deserving of special recognition for helping me through the abyss of a 3,300 mile move.

Professor Vermeulen's guidance and infinite patience were instrumental in overcoming obstacles both real and imagined.

Finally, I would like to express my deep appreciation to an American educational system that has allowed me to grow in ways that I never conceived of seven years ago. This has been manifested in all my experiences at Berkeley, which are certain to become more meaningful to me with the passage of time.

This work was prepared with the support of the U. S. Department of Energy under Contract No. W-7405-ENG-48.

Multiphase Reactor Modeling for Zinc Chloride Catalyzed Coal Liquefaction

Peter James Joyce

Energy and Environment
Lawrence Berkeley Laboratory
and Department of Chemical Engineering
University of California
Berkeley, California 94720

ABSTRACT

A generalized reactor design is presented for a low-temperature coal-conversion method, where coal is slurried in an 83 wt% zinc chloride methanol melt and allowed to react at moderate conditions of 275^{o}C and 600 psi hydrogen. The hydrogen being sparged countercurrently at five levels. In the reactor, the slurried melt flows downward in plug flow on the order of 1 foot per minute through a distance of 15 feet.

Model-liquid mass-transfer studies have been undertaken to examine specific effects of zinc chloride in a viscous medium, in order to determine the rate-limiting step in the overall hydrogen absorption rate. The absorption rate can be expressed in terms of a resistance-in-series model. These experiments, interpreted in terms of existing well established correlations involving especially the effects of viscosity, have shown that the use of zinc chloride introduces no new effects and that the chemical reaction rate of the coal particle is controlling.

I. Introduction

The need to develop new coal liquefaction technology in the United States is manifested in two unrelated problems pertaining to the present energy picture. They are the escalating cost of our foreign oil supply and the poor thermal efficiency obtained from state-of-the-art coal liquefaction processes. The supply and cost of imported petroleum products are unpredictable--a fact acutely borne out by recent political upheavals in the Middle East, and by the 1973 and 1979 quantum jumps in OPEC oil prices demonstrating that the selling price of crude bears little relation to the cost of production.

A typical coal liquefaction plant during the 1990's will process 25,000 tons of coal per day (C2) in order to recover 75,000 barrels of oil. The enormity of the investment and the lead time requirement dictate that all potential processes be carefully scrutinized now so as to insure that the most economic process is employed to deliver coal-derived liquids to the domestic market.

A. Coal Liquefaction Overview

None of the three high temperature coal liquefaction processes, listed in Table I-1, are ready for commercial implementation. The farthest along is the Exxon Donor Solvent process, which will be employed in a 250 ton/day pilot plant scheduled to go on stream in 1981 (E1). Hydrogen is added to ruptured coal fragments through a tetralin-rich donor solvent. After having donated its excess hydrogen, the tetralin is recycled to a unit where it is rehydrogenated by a catalyst. Hydrocarbon Research Institute is working on the H-Coal coal liquefaction process, where coal is slurried in "anthracene oil" (recycle solvent)

and treated with hydrogen while in contact with a solid catalyst, cobalt molybdate (H1).

Keeping the coal in a simpler reacting scheme differentiates the Solvent Refined Coal (SRC-I and SRC-II) processes from the previously mentioned ones (A3). Here the coal is dissolved in a hot recycle solvent and heated to reaction temperature. A solid product low in sulfur content is obtained from SRC-I. SRC-II differs in that it mixes part of the liquid product stream with the recycle solvent. This results in higher liquid yields.

Severe operating conditions, unfortunately, characterize all of these processes. This limits the amount of recoverable energy from coal, and adds to the the unit cost of the final product. An improvement over these temperatures and pressures would have a profound positive impact on the process economics.

Table I-1. Operating conditions of present coal liquefaction processes.

Process	Temperature °C	Pressure psi
Exxon Donor Solvent	400-480	1500-2500
H-Coal	450	2800
Solvent and Refined Coal, I and II	440	2000-3000

B. $ZnCl_2$-Catalyzed Coal Liquefaction

1. High Yield Batch-Reactor Results

Coal conversion at relatively mild temperatures, 275°C, and moderate hydrogen pressure, 500 psi, has been demonstrated by Holten (H5) and reported by Shinn (58,59) at Berkeley. Within 30 minutes a 50% conversion of coal occurs to oil and "asphaltenes" with another 40% converted to pyridine-soluble "preasphaltenes". The main advantage of this technique is that it selectively cleaves ether (carbon-oxygen) and aliphatic (carbon-carbon) bonds which crosslink the coal structure. The product from this treatment is expected to lend itself to upgrading to liquid petroleum products by current refining technology.

2. $ZnCl_2$/MeOH Coal Liquefaction Process Design

A possible process design based on the low temperature coal conversion scheme is shown in Figure I-1. Raw coal is blended into a slurry with $ZnCl_2$ and methanol at 175°C and 1 atm, pumped to 35 atm, heated to 275°C, and fed continuously to the top of a plug flow reactor in which it is contacted countercurrently with a mixture of recycled and fresh hydrogen that is sparged in at several levels along the height of the reactor.

The reactor is divided into two reaction zones of 275°C and 325°C. It is believed that the higher final reaction temperature will complete the conversion of preasphaltenes to liquid products. Initial coal conversion is largely due to the breaking of ether linkages, while complete conversion also requires breaking C-C and perhaps C-N linkages. The higher temperature is needed to obtain a reasonably constant rate of hydrogen uptake and coal conversion. Between the two reactor zones

the gas leaving the 325°C section may be scrubbed to remove H_2O which has a significant vapor pressure under these conditions (H5). The cross-hatched patterns in the reactor sections represent internals installed to break up the flow of melt and increase the interfacial area for hydrogen absorption. Within the reactor they are arranged in a stacked pattern with each succeeding tray turned at a 90° angle to the previous one. This type of reactor internal is not unlike the turbogrid distillation tray introduced by Shell Development Company (T2).

From the reactor the solubilized coal, unreacted coal, ash and $ZnCl_2$/MeOH melt may then move by gravity into an extraction column where countercurrent flows of recycle solvent extracts the bulk of the reaction product. (If the product self-separates, extraction may not be needed.) The melt then proceeds downward to a settler where phase separation takes place, allowing a slip stream of $ZnCl_2$ melt to be removed with the ash, purified, and recycled; the main $ZnCL_2$ layer (containing some incompletely reacted coal) to be directly recycled; and the organic layer to be returned to the extraction stream or combined with the extract.

Plug flow of slurried melt has been chosen for the conceptual design, because it should give shorter residence times, better process control, and fewer mechanical problems than stirred vessels singly or in series. In the work of Shinn and Vermeulen, hydrogen contacting was not a problem, because stirring provided the needed interfacial area. However, in the proposed contacting scheme, limitations on the chemical reaction rate could arise from a slower rate of mass transfer in the slurried melt. This concern has made it necessary to carry out experiments to assess the flow behavior and the mass transfer rates.

COAL TO OIL
(Conceptual design)

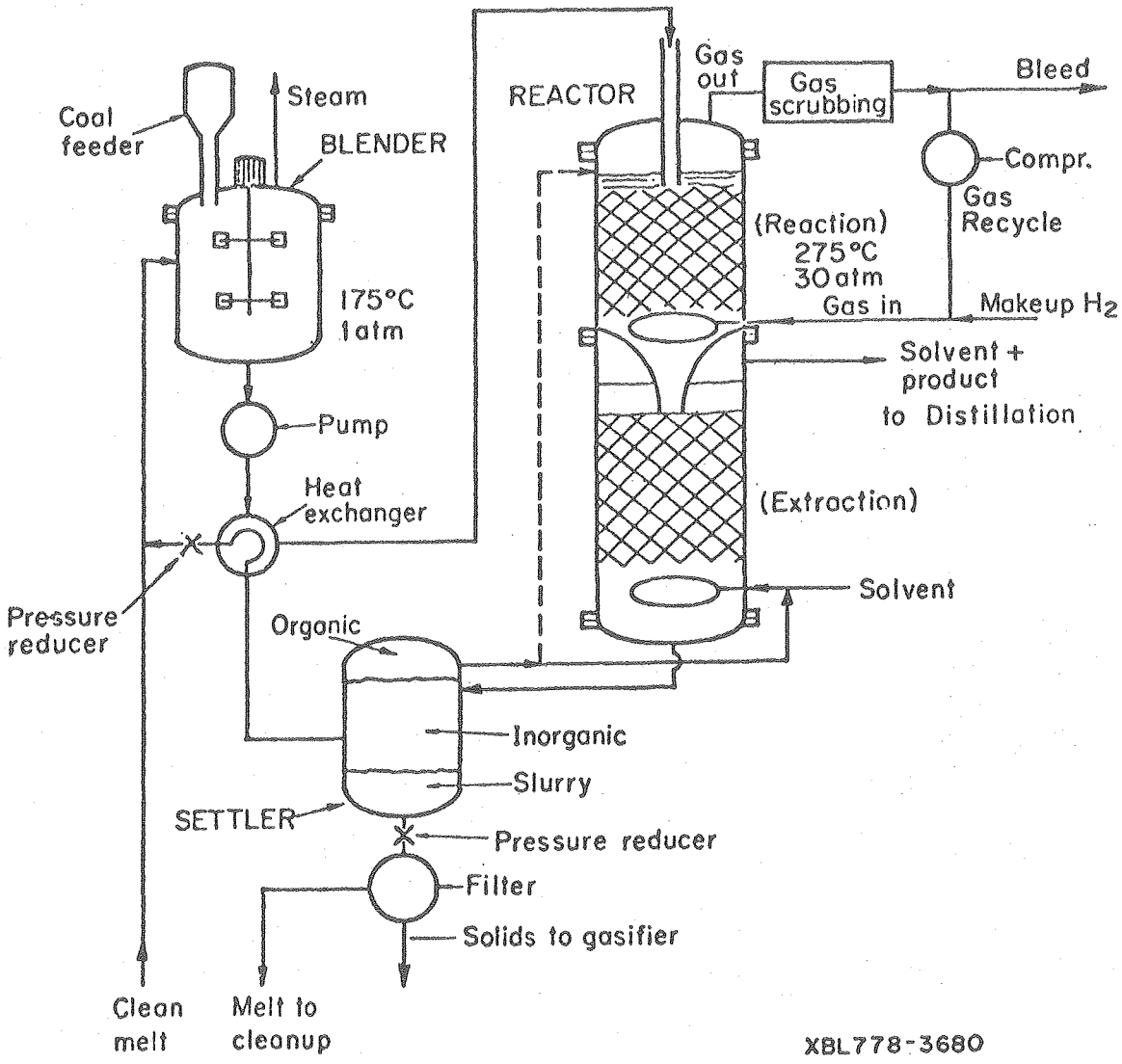

Figure I-1. Conceptual Low Temperature Coal Conversion Process Design.

C. Project Objectives

In summary there are three goals of this study. The first is to evaluate the design of a proposed coal liquefaction reactor commensurate with the unique reaction conditions of the low-temperature melt-catalyzed process. The second is to carry out experimental measurements in a "cold model" of a reactor section that will yield representative design data applicable to a three phase coal-liquefaction slurry reactor employing a $ZnCl_2$ melt. For exact anlysis the data will need to be corrected for temperature, pressure, gas composition, and melt-slurry viscosity not known precisely at reaction conditions, being a function of conversion and temperature. An upper bound on viscosity will be assumed, so that its effect can be allowed for. Other variables studied include gas flow rate, the configuration of the reactor internals, solids loading, and sparger design. Finally, this study can be used as a guide for systematic research for slurry reactors in general and coal liquefaction reactors in particular. The literature is lacking in many areas with respect to two and three phase systems and a research attack method for the design engineer is warranted. Thus, by starting with a two phase system and increasing the complexity by adding solids, and then again by having a chemical reaction, a fundamental understanding of a slurry reactor will emerge.

Like any other initial design, the present study will make it possible to identify further areas of research needed in the development of these new coal liquefaction conditions.

II. Slurry Reactors

A. Studies Related to Commercial Coal Liquefaction

Among the three currently projected liquefaction processes mentioned above, the Exxon development has included the use of design data from a room temperature model, leading to estimates of hydrogen consumption rate which is based partly on a correlation from Calderbank (C1). In comparing this rate with the chemical reaction rate, the Exxon investigators noted that mass transfer could conceivably offer an additional resistance. However, the correlation makes no allowances for the presence of solids which has been shown by Joosten (J2) to decrease the volumetric mass transfer coefficient in a slurry of polypropylene beads. Misic (M5) reports that at the same particle size in a carbon slurry the presence of solids had no effect. It is important to note that Joosten used a stirred gas-liquid contactor while Misic employed a Pyrex gas washing bottle for his experiments, and that both are well removed from a bubble column slurry reactor.

A study on contacting in the Synthoil coal liquefaction process, which is not now under active development, was done by Javdani et al (J1). Here the slurried coal was reported to behave like a homogeneous Newtonian liquid, the coal particles being less than 177 μm in diameter and their specific gravity 1.1 gm/cm^3. Their data showed that the gas-phase holdup decreases with increasing coal concentrations.

A fundamental analysis of actual run data for coal liquefaction has been reported by Wen (W2). He proposed a first-order dependence of the coal dissolution rate and hydrogen absorption rate on unreacted coal, based on information from the SRC, Synthoil, and H-Coal processes,

and found that the coal-dissolution rate constant for coal liquefaction in "creolite oil" at 450°C is proportional to the square root of the hydrogen partial pressure, implying a combination of intraparticle mass transfer and chemical reaction.

Wen (W3) also determined an overall absorption coefficient that takes into consideration the effect of mass transfer. Fundamentally the problem was set up correctly in choosing a driving force from the gas phase to the bulk liquid. However, it was assumed erroneously that the driving force was constant, i.e. that the equilibrium back pressure of H_2 in the liquid did not change as a function of position within the reactor. If the coal concentration can be assumed to be in excess and the hydrogen pressure in the gas phase is in equilibrium with the liquid, i.e. the mass transfer rate is large, then the absorption coefficient reported is in essence the chemical reaction rate constant at the coal particle surface. The differential equation relating the change in hydrogen partial pressure with time should show that what is being measured is the change in <u>equilibrium</u> pressure with time. This development assumes the liquid-solid mass transfer coefficient is negligible in comparison. For the H-Coal process $K_{og}a$ was found by Wen to be 11×10^{-5} gmole/hr-cm^3-atm at 450°C. The activation energy of 27.6 kcal/gmole is another indication that the rate is partly chemical rate controlled. The activation energy reported by Shinn at 800 psig and 275°C is also 28 kcal/gmole but such agreement is probably a coincidence.

B. Experimental 3 Phase Reacting Systems

Among the more relevant three-phase reactor studies, Sherwood and Farkas (S6) carried out experimental hydrogenation runs in a bubble-column slurry reactor for three different reactants-- methyl styrene, ethylene, and cyclohexene. By measuring the reaction rate for a varying weight fraction of solids, they were able to show that the liquid-solid mass-transfer resistance was greater than the chemical reaction rate, a valuable result with respect to apparatus design.

Much experimental work has been done on slurry reactors with respect to removal of sulfur dioxide from air (S1, G2, K5). Sada et al. (S1) extended the mathematical model of Uchida et al. (U1) to SO_2 removal from flue gas, taking into account the slow second order chemical reaction rate. Goto and Smith (G2) compared a continuous stirred-tank slurry reactor and a trickle-bed reactor for their ability to remove SO_2. In this mathematical model they relaxed the assumption of plug flow of gas bubbles, and solved the differential equations for the well-mixed case. Experimental results showed that per unit weight of carbon catalyst the slurry reactor removed more SO_2 than the trickle-bed reactor, through the use of smaller particles. Their slurry-reactor data were obtained from an earlier study by Komiyama (K5), who had shown that the rate-controlling step was the adsorption of oxygen on the carbon particles.

Other experimental studies of a three-phase slurry reactor were done by Juvekar and Sharma (J3) on the absorption of carbon dioxide in a lime slurry, and by Niyama and Smith (N1) on the absorption of nitric oxide in an activated carbon slurry.

C. Two and Three Phase Nonreacting Systems

In designing a 3 phase reactor the most important parameters with respect to mass transfer are melt viscosity, surface tension, particle size, liquid-solid density ratio, and solids concentration. At a constant superficial gas velocity they have the strongest effect on the turbulence attainable within the reactor and hence the rate of mass transfer.

The complexity of contacting systems increases in going from a two-phase gas-liquid bubble column to a three-phase system containing added solids, and increases again in allowing a chemical reaction to take place in the three-phase system. The investigations of the simpler systems is highly significant for understanding the complex interactions of variables in the slurry reactor. In particular, two-phase gas-liquid flow systems have been widely studied, so much so that a literature review up to 1966 by Gouse (G3) covered more than 5,000 references.

Slurry reactor research should start with a fundamental understanding of the gas-liquid system being used and then build in complexity with the physical effects of the solids and chemical reaction. In each slurry reactor development the experimental and theoretical research is then compared against the literature and integrated into the next design step. A conceptual picture of this research approach is shown in Figure II-1. Table II-1 lists the variables whose effects must be understood during each level of the design development. In the technical literature the effects of the two-phase variables are well established. However, for bubble columns the effects of small particles, surface tension, surfactants, etc. are dealt with sparingly

for three-phase systems and not at all for slurry reactors. Thus, while certain regimes of three-phase reactors have been studied in detail, the need for a grass roots approach, to this author's knowledge, has not been addressed.

The most extensive and useful studies of mass-transfer in a two-phase gas-liquid contactor was reported by Yokita and Ashida (Y1, A1, A2). They have studied the gas-liquid mass transfer rate as a function of gas and liquid properties and hydrodynamic conditions within the column, using a sulfite-oxidation technique and the liquid being charged in a batch mode. They report volumetric and true liquid-side coefficients as a function of superficial gas velocity, using liquid viscosity, column diameter, bubble diameter, and surface tension as correlating parameters. Their experimental results showed that

1. Even at low superficial gas rates, the liquid can be considered to be well mixed locally.
2. Gas phase resistance is negligible; changing from oxygen to air had no effect on the volumetric mass-transfer coefficient.
3. Gas phase holdup and volumetric mass-transfer coefficient remain unchanged over an order of magnitude increase in gas-inlet orifice diameter, for orifice flowrates between 1.75×10^{-3} and 1.40×10^{2} cm^3/s.
4. Gas density has negligible effect with respect to holdup.
5. The liquid film coefficient, k_l, is inversely proportional to the one-half power of bubble diameter.

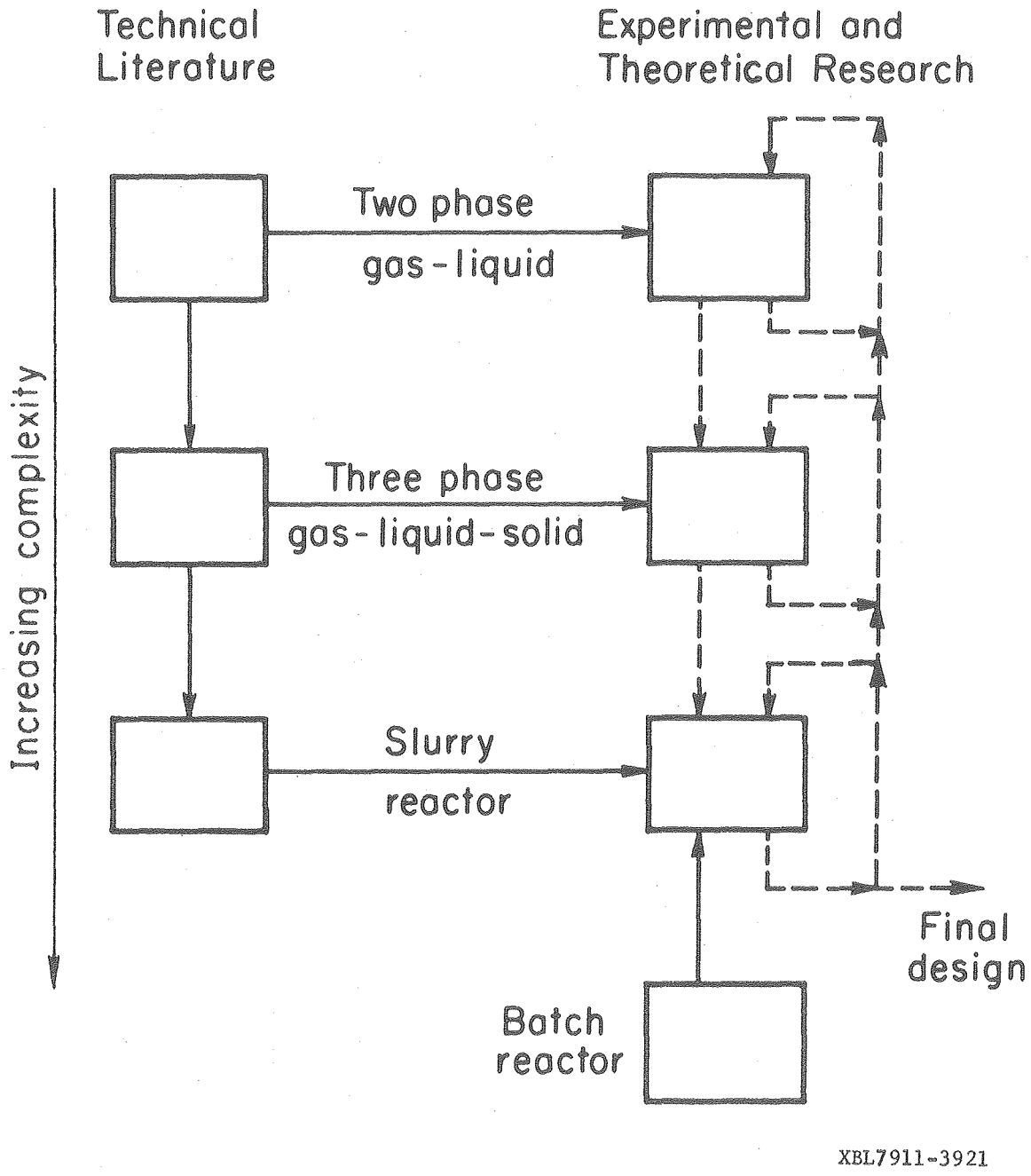

Figure II-1. Suggested approach to slurry reactor research.

Table II-1. Variables whose effects must be considered in the complete design of a slurry reactor.

INDEPENDENT VARIABLES
1. System Physical Properties
Gas-Liquid
Melt Viscosity, Surface Tension, Diffusivity, Surfactants, Gas Composition, Henry's Law Constant
Gas-Liquid-Solid
Slurry Viscosity, Particle Size, Solids Concentration, Liquid-Solid Density Ratio
Slurry Reactor
Chemical Reaction
2. Hydrodynamic and Operating Variables
Temperature, Pressure, Gas and Slurry Flowrates, Reactor Internals, Sparger Design, Column Diameter
DEPENDENT VARIABLES
Bubble Size, Phase Holdups, Phase Circulation, Absolute and Relative Mass Transfer Rates, Overall Conversion, Pressure Drop

Yokita and Ashida took photographs of bubble swarms, and presented a correlation for the average bubble size as a function of superficial gas velocity and of liquid physical properties. This average bubble size can be used with holdup data to determine the interfacial area available for mass transfer.

Towell et al. (T1) in a mass-transfer study of very large columns concluded through tracer tests that the liquid phase is locally well mixed and the gas-phase is in plug flow. They determined three distinct regions for holdup within the column. First, very close to the sparger there is jetting action of the gas. Next, in an extended middle region of the column, coalescence and breakup rates balance each other and the holdup is larger. Third, near the surfce, bubbles coalesce, and the holdup is again smaller.

Bhavaraju et al. (B1) stress the existence of an area of lean holdup near the sparger in a gas-liquid contactor. They develop a potential-flow model for liquid circulation pattern near each individual orifice in a sparger, to predict at what height above the orifice the liquid becomes turbulent and produces a greater holdup. Because spargers are scaled up by increasing the number of orifices, the changeover occurs at a fixed height and is not proportional to the equipment scale.

Mashelkar (M2) found that the values of $k_l a$ and holdup are not dependent on the liquid flowrate for moderate superficial liquid velocities. However, he found that the liquid was not completely mixed and correlated his data and Towell's using an axial diffusion model that brought the two into close agreement.

In several studies the effect of column diameter on gas holdup has been found to be negligible for columns larger than 7.5 cm (H6, E2, M2). The effect of viscosity on volumetric mass transfer coefficient is complex; increasing the viscosity increases the interfacial areas available for transfer (S5), but decreases the liquid mass-transfer coefficient due to decreased diffusivity, and terminal velocity.

Calderbank (C1) states that in aerated mixing vessels the mass transfer coefficient is independent of bubble size and depends only on the physical properties of the system. He presents correlations for two bubble sizes and identifies a transition regime between "small" and "large" bubbles. The small bubbles, on the order of 1 mm behave like rigid spheres. He also notes that the relative velocity between solids and liquid is retarded as in boundary layer theory and does not use particle size as one of the correlating parameters.

Hughmark (H6) presents correlations for single gas bubbles and for bubble swarms. He uses the same form of the equation in both cases but changes the coefficient on the correction term from Stokes Law where the Sherwood number is 2. This correction says that mass transfer for bubble swarms is less than that for single bubbles at the same diameter, bubble rise velocity and liquid physical properties. This is contrary to the belief that liquid turbulence, which would be increased with bubble swarms, increases mass transfer.

Higbie (H3) was the first to derive an expression for the liquid side mass transfer coefficient by solving the unsteady state differential equation for mass transfer into a semi-infinite medium. The contact

time he used was the time it takes a bubble to rise one bubble diameter or the rise velocity divided by the bubble's diameter.

Table II-2 presents correlations obtained by these authors for liquid-phase mass-transfer coefficients.

The most extensive work in a three-phase gas-liquid-solid system was done by Kim et al. (K2, K3, K4). They obtained phase holdup data in a three phase system for a wide range of superficial gas velocities, particle sized, and liquid properties. Their data led to the following conclusions.

1. The steady state bed volume decreased upon gas injection, owing to the formation of solid-free liquid wakes behind the bubbles.
2. Particle size does not seem to affect bubble size, in contrast with other investigators.
3. With small-diameter particles (1 mm or less) three phase beds exhibit a narrower bubble-size distribution than two-phase beds.
4. Increasing particle size increases gas holdup, decreases bed expansion, and axial mixing. The holdup effect is due to smaller bubble rise velocity and smaller bubble diameter.
5. Gas holdup was not a strong function of liquid rate.
6. At low gas rates the influence of solids on bed hydrodynamics is small.
7. At high gas flowrates and correspondingly large bubble sizes (5 cm), the influence of liquid viscosity on bubble characteristics for all particle sizes (1 to 6 mm) is relatively small.

Table II-2

Correlations For Liquid Phase Mass Transfer Coefficients

Correlation	Reference	Comments
$k_l(N_{Sc})^{1/2} = 0.31\ (\frac{\Delta\rho\mu_c g}{\rho_c^2})^{1/3}$	C1	Bubble diameters less than 0.1mm
$k_l(N_{Sc})^{1/2} = 0.42\ (\frac{\Delta\rho\mu_c g}{\rho_c^2})^{1/3}$	C1	Bubble diameters greater than 2.5mm
$\frac{k_l a D_c^2}{D} = 0.6\ (\frac{\nu_l}{D})\ 0.5\ (\frac{gD_c^2}{\alpha})\ 0.62\ (\frac{gD_c^3}{\nu_l^2})\ 0.31\ (\epsilon_g)^{1.1}$	A1	7-60 Column Diameter U_g = 0.7 to 24.2 met/min Viscosity of 1-7 cp
$N_{Sh} = \frac{k_l d_b}{D} = 2 + 0.0187\left[(N_{Re})^{0.484}(N_{Sc})^{0.339}\frac{d_b g^{1/3}}{D^{2/3}}\right]^{1.61}$	H5	For Bubble Swarms, (For Single Bubbles Change 0.0187 to 0.061)
$k_l = (\frac{4\pi D v_b}{d_b})^{1/2}$	H2	Higbie Penetration Model

8. At high liquid viscosity, gas holdup is higher in a three phase bed than in a two phase bed.
9. In a three phase system, bubble size and rise velocity increase with increasing superficial gas velocity.

Kim makes a case for discarding the well known equation for gas holdup in a three phase system

$$\varepsilon_g = U_g/v_b$$

where U_g is superficial gas velocity and ε_g is fractional gas holdup

This equation assumes equal-volume uniformly spaced bubbles rising at uniform velocity. This, he says, is not true due to the establishment of preferred paths by the three phases within the column. He suggests this as an area of further research.

Darton and Harrison (D1) confirm Kim's contention of a bed contraction with gas injection and correlate their data in terms of the ratio of liquid wake volume to bubble volume.

Sharma et al. (S5) report that the presence of solids affected coalescence, causing a smaller bubble size and larger interfacial area. He also found that solids interfere with interfacial turbulence, so that the resulting decreased interfacial mobility decreased the liquid mass transfer coefficient. Thus the combined effect is not as great as either one alone on the volumetric mass-transfer coefficient.

Rigby et al. (R4) obtained data on bubble sizes and rise velocity in three-phase beds using an electrosensitivity probe. The probe consisted of two 0.5 mm diameter chromel alumel electrodes which were aligned vertically 0.85 cm apart. It was housed in a glass assembly and could be

positioned anywhere within the bed. A voltage drop fluctuating between 0 and 1 volt occurred between the wall electrode (consisting of copper strips cemented to the wall) as the circuit between the two was opened and closed. They varied liquid and gas superficial velocity and particle size. The liquid and gas were in cocurrent flow and the solids were loaded in the batch phase. Their data show that

1. Radial distribution of bubbles for a three-phase system is similar to that of a two phase system.
2. Bubble size increases with height above the distributor as well as with decreasing liquid rate or increasing gas rate.
3. Bubble coalescence is less frequent in three phase beds than in two phase beds.

Rugby et al. (R4) also present a correlation of bubble velocity as a function of gas flow rate, bubble length, and bed porosity, the latter being defined as the sum of gas and liquid holdup in a three-phase bed.

Razumov et al. (R3) present correlations of liquid holdup for four different particle sizes as a function of liquid and gas superficial velocities.

D. Slurry Reactor Theory

1. General

Slurry reactors have been an area of considerable theoretical investigation. Govidaro (G3) solved the basic differential equations for the transient response of a bubble-column slurry reactor to a step change in gas or liquid concentration. The chemical reaction was first order and irreversible and was assumed to take place on the particle surface.

Ramachandran and Smith (R2) were interested in the relative magnitude of the various coefficients and their impact on performance. They were able to identify the effects of first-order kinetics, reversible adsorption at the particle surface, gas-liquid and liquid-solid mass-transfer coefficients, and intraparticle diffusion. Their method of measurement was the system response to a step or pulse input.

Uchida and Wen (U1, U2) present a clear description of the overall absorption rates as a function of three criteria:

1. Where is the reaction plane located? Does the assumedly instantaneous reaction occur in the gas-liquid or liquid-solid film?
2. Does solid dissolution in the gas-liquid film enhance the absorption rate?
3. Is the liquid phase saturated with the dissolving solid phase?

The results were applied to the rate of limestone dissolution in a sulfur dioxide scrubber.

2. Application to $ZnCl_2$/MeOH System

The following is a series-resistance approach for predicting the rate of hydrogen consumption in a through-flow coal-liquefaction reactor using the low-temperature melt-catalyzed reaction conditions. The rate expression to be developed is based on four assumptions.

1. The liquid phase is locally well mixed, so that there is no resistence in the bulk liquid.
2. Coal particles dissolving in the liquid film do not enhance the absorption rate (see Appendix B).

3. The chemical reaction rate is first-order in hydrogen and unreacted coal.
4. Intraparticle diffusion is included in the apparent chemical rate.

The assumption that the reaction is first-order in hydrogen comes from earlier kinetic studies of coal liquefaction in $ZnCl_2$ media (G6, S11) as well as from Shinn. A representative plot from Shinn (S9) of pressure drop vs. time, corrected for competing reactions, is given in Appendix E; assumption 4 can be inferred from these data.

The rate of hydrogen absorption can be expressed in terms of four distinct resistances and their associated coefficients. Thus at any horizontal cross-section within the reactor the volumetric rate of hydrogen consumption, R, can be expressed as (S4)

Rate expression	Regime of Transfer
$R = k_g a\ (C_g - C_{1g})$	Bulk gas to gas-liquid interface
$k_l a\ (C_{il} - C_l)$	Gas-liquid interface to bulk liquid
$k_s a_p\ (C_l - C_s)$	Bulk-liquid to coal particle surface
$k_r\ C_s$	Chemical reaction inside particles

A schematic diagram of these resistances is shown in Figure II-2. If the gas at the gas-liquid interface is in equilibrium with the liquid at the interface, and hydrogen solubility is assumed low, then Henry's law holds

$$C_{ig} = HC_{il} \quad \text{and} \quad C_g = HC_g^*$$

The rate of hydrogen consumption in lb moles per unit volume of melt coal slurry can be expressed in terms of a global coefficient and the equilibrium liquid-phase hydrogen concentration as

$$R = K_o C_g^*$$

and

$$\frac{1}{K_o} = \frac{1}{Hk_g a} + \frac{1}{k_l a} + \frac{1}{k_s a_p} + \frac{1}{k_r \eta}$$

It is necessary, then, to measure experimentally, or to calculate from existing correlations, all of the above coefficients in order to ascertain which resistance is controlling. A room-temperature experimental model without reaction was developed to obtain $k_l a$. The information so obtained can be adjusted for temperature and pressure for ultimate use in the final design.

The injection of hydrogen at five discrete levels along this reactor makes it necessary to carry out a material balance on each station. In order to size any one section, three assumptions are made

1. The liquid is well mixed.
2. The gas rises in plug flow.
3. An average coal concentration can be assumed in any one section so that the chemical rate constant is first-order in hydrogen.

The major design consideration is the amount of hydrogen required to react with unit mass of coal or unit mass of slurry. Excess hydrogen is fed to each reactor section, but the maximum coal convesion that occurs within any one section is 25%. For each section an average value

of unconverted coal is assumed to apply. If K_o for the section is calculated for the average interfacial area in the section, the reaction rate in the section becomes effectively zero-order, for constant hydrogen pressure.

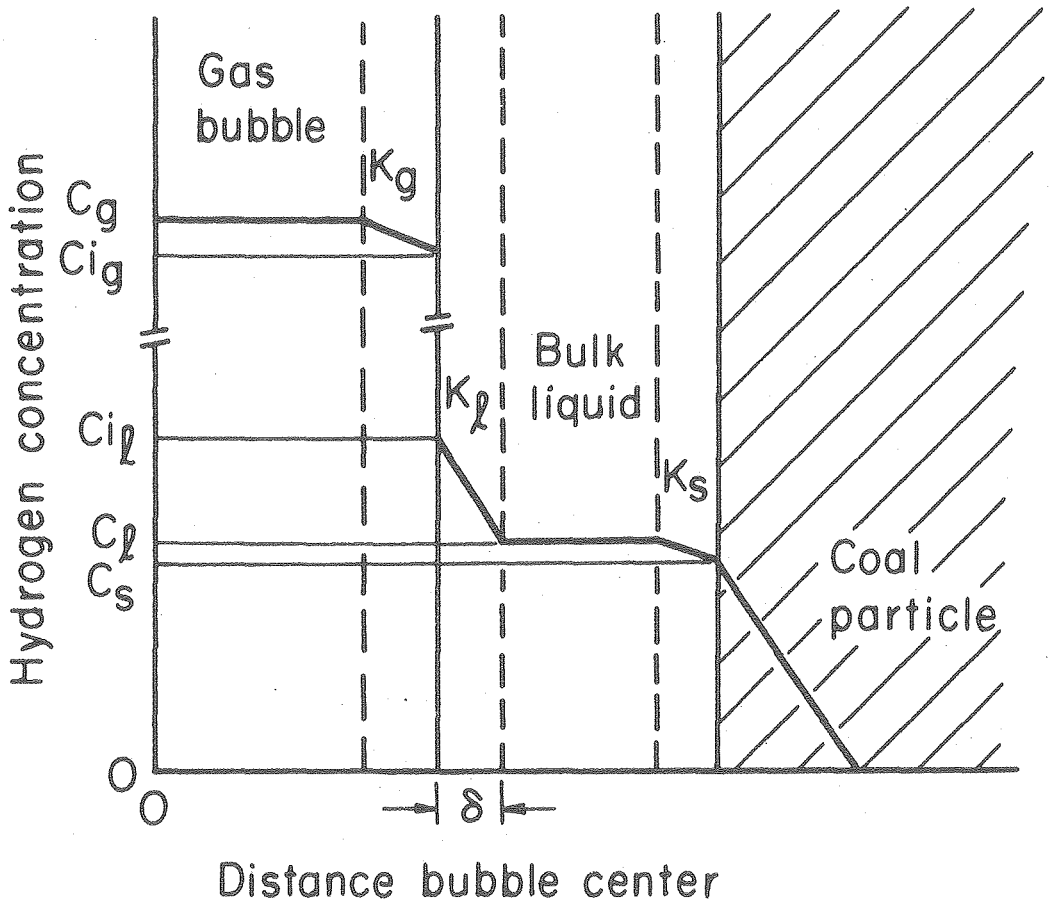

XBL7910-3872

Figure II-2. Mass-transfer resistances in coal liquefaction.

III. Materials and Equipment

Table III-1 lists the components and physical properties of the liquids employed to model the behavior of the $ZnCl_2$/Coal melt used in the Berkeley process. At 250°C the melt has an assumed viscosity of 0.6 cp (Appendix A). According to Einstein's formula for solids influence on viscosity, the addition of 30 wt% small coal particles should increase that viscosity to around 10 cp. By increasing the viscosity by another order of magnitude, its effect can be completely bracketed.

A. Status Equilibrium Apparatus

Figure III-1 depicts the equipment flowsheet used to obtain mass-transfer coefficients for the n-propanol system and gas holdup for these liquids. The apparatus could be operated in one of two modes, depending on whether equilibrium or mass-transfer data were desired. In either case, nitrogen was fed through rotameters to the column under study and passed through heated lines to the gas chromatograph. A vent valve close to the chromatograph and a 6-port flow-through gas sample valve enabled the gas flowrate in the 1/8-inch transfer lines to be kept as high as possible. Also, a time interval equal to 3.5 retention times was allowed between samples. These two precautions ensured that the gas being analyzed was the same as that in the column. The mass-transfer column was fed with a Fischer and Porter model 1/2-G17-10/83 rotameter, and the equilibrium column with a Dwyer Instruments type-190975 rotameter. In all equilibrium runs the flowrate was constant at 1000 cm^3/min. The transfer lines, gas sample valve, and sample loop were all heated to 75°C to ensure that no condensation occurred.

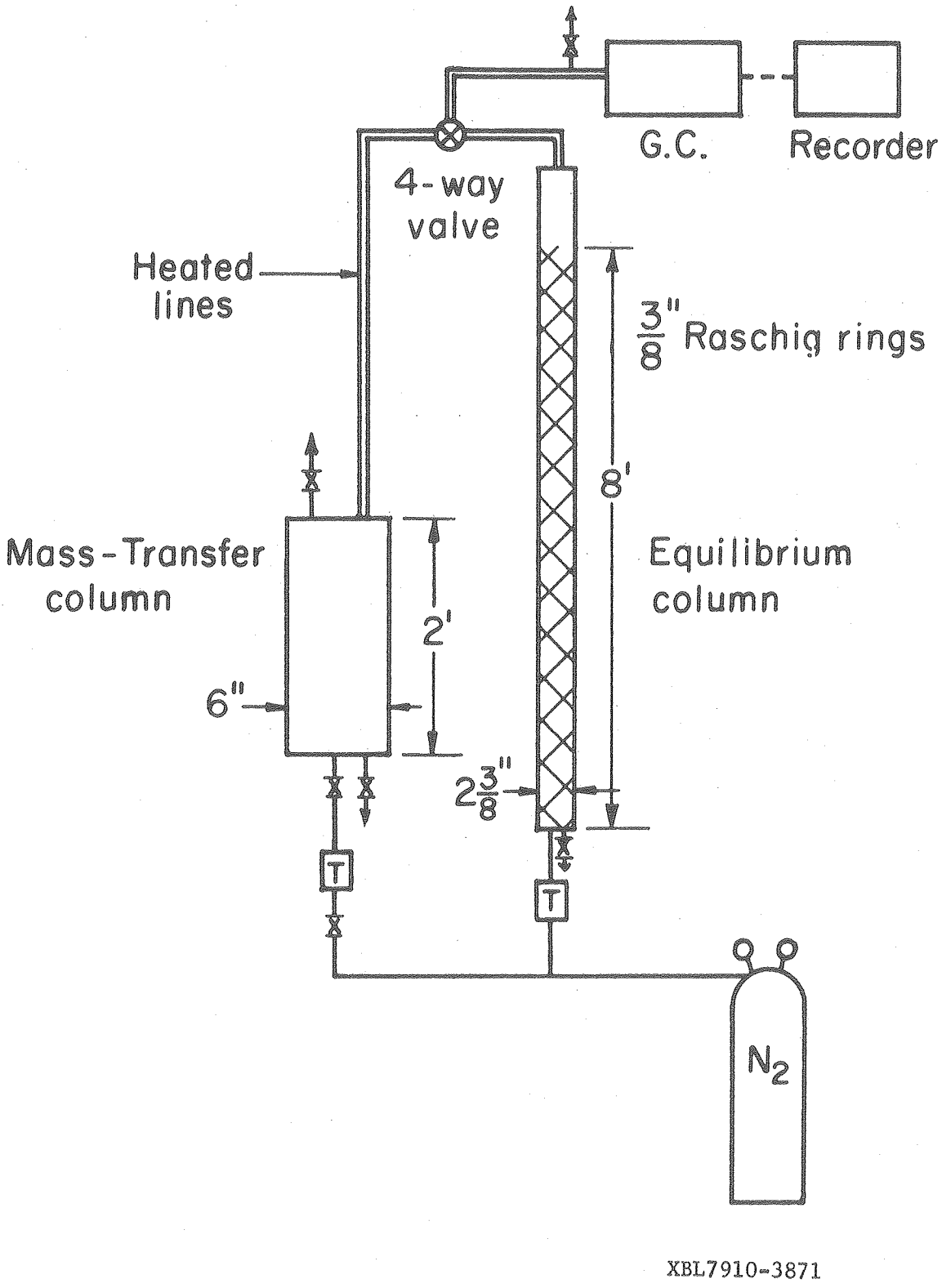

Figure III-1. Static Equilibrium Apparatus.

Table III-1

Liquids Used to Model $ZnCl_2$/MeOH Melt

	A		B		C	
Viscosity, cp	84		22		1	
Surface Tension, dynes/cm.	67		76		64	
Density gms/cm^3	1.46		1.37		1.2	
	Wt%	Mole%	Wt%	Mole%	Wt%	Mole%
Component						
$ZnCl_2$	30.7	12.3	38.7	11.1	20.0	3.2
J_2O	18.7	56.8	36.0	78.1	80.0	96.8
Glycerol[a]	47.5	28.2	20.8	8.8		
n-Propanol[b]	3.0	2.7	3.0	2.0		

a Matheson-Colemen-Bell Technical Grade

b J. T. Baker Reagent Grade

The gas chromatograph (Model A-90) and accompanying gas sample valve were manufactured by Varian Instruments. The operating conditions and column employed are described in Table III-2. In order to reduce end effects, which presumably led to the observed attainment of equilibrium within the column, it was necessary to weld the inlet valve to the bottom flange. This kept liquid from dripping down the feed line which appeared to cause significant mass transfer outside the column.

Table III-2. Operating conditions for gas chromatograph for n-propanol experiments.

Column Packing	Chromosorb 104
Column Dimensions	6 ft by 0.25 inch diam.
Carrier Gas	Helium @ 75 cc/min
Oven Temperature	195°C
Detector Temperature	205°C
Injector Temperature	150°C
Filament Current	200 ma

At the top liquid surface, end effects were minimized by installing a gas-collecting cone, shown in Figure III-2, that allowed N_2 bubbles to be collected below the liquid level. This reduced splashing and dead volume effects, both of which could also cause extraneous mass transfer. The cone consists of an inverted glass funnel with a rubber stopper that admitted the sample line. A union close to the stopper enabled the height of the cone to be adjusted, along with the liquid level. Tight

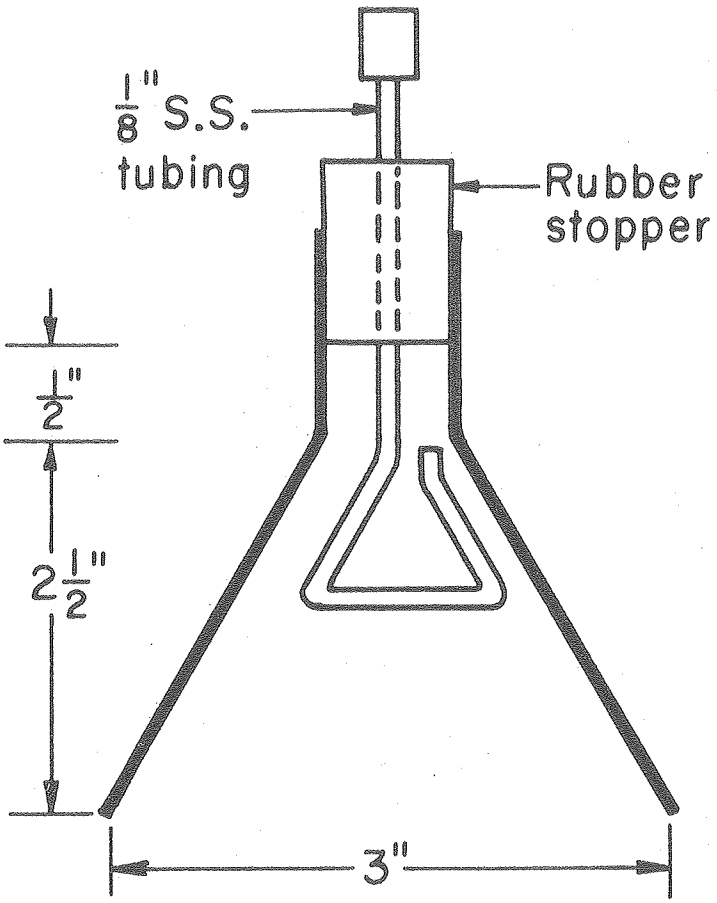

XBL7910-3870

Figure III-2. Gas collecting cone.

connections from the cone through the top of the column completed the sample train to the heated transfer lines and the gas chromatograph. The vent valve on the top flange was opened slightly to keep the pressure from building to the point where liquid would be forced into the sample line.

Figure III-3 shows a gas sparger used in the gas holdup experiments. It consists of thin parallel disks, bottom fitted with a 3/8-inch internal pipe thread, fitting a nipple welded to the bottom flange. Use of a 3/8-inch orifice in certain runs simply indicates that sparger-less operation is being used.

Figures III-4 and III-5 show top and side views of a 1/4-inch and a 1/2-inch rod tray that were considered as internal packings suitable for use with a slurry. They will maintain uniform slurry flow and gas flow throughout any column cross section, and may possibly increase the interfacial area available for mass transfer. The rings were cut from 6-inch Plexiglas pipe and turned on a lathe to fit snugly into the column. Saw tooth cuts were then made in them to provide for installation of evenly spaced rods. When the rod-trays were stacked in the column each tray was turned 90^{o} to the adjacent one so that alternating trays had parallel rods.

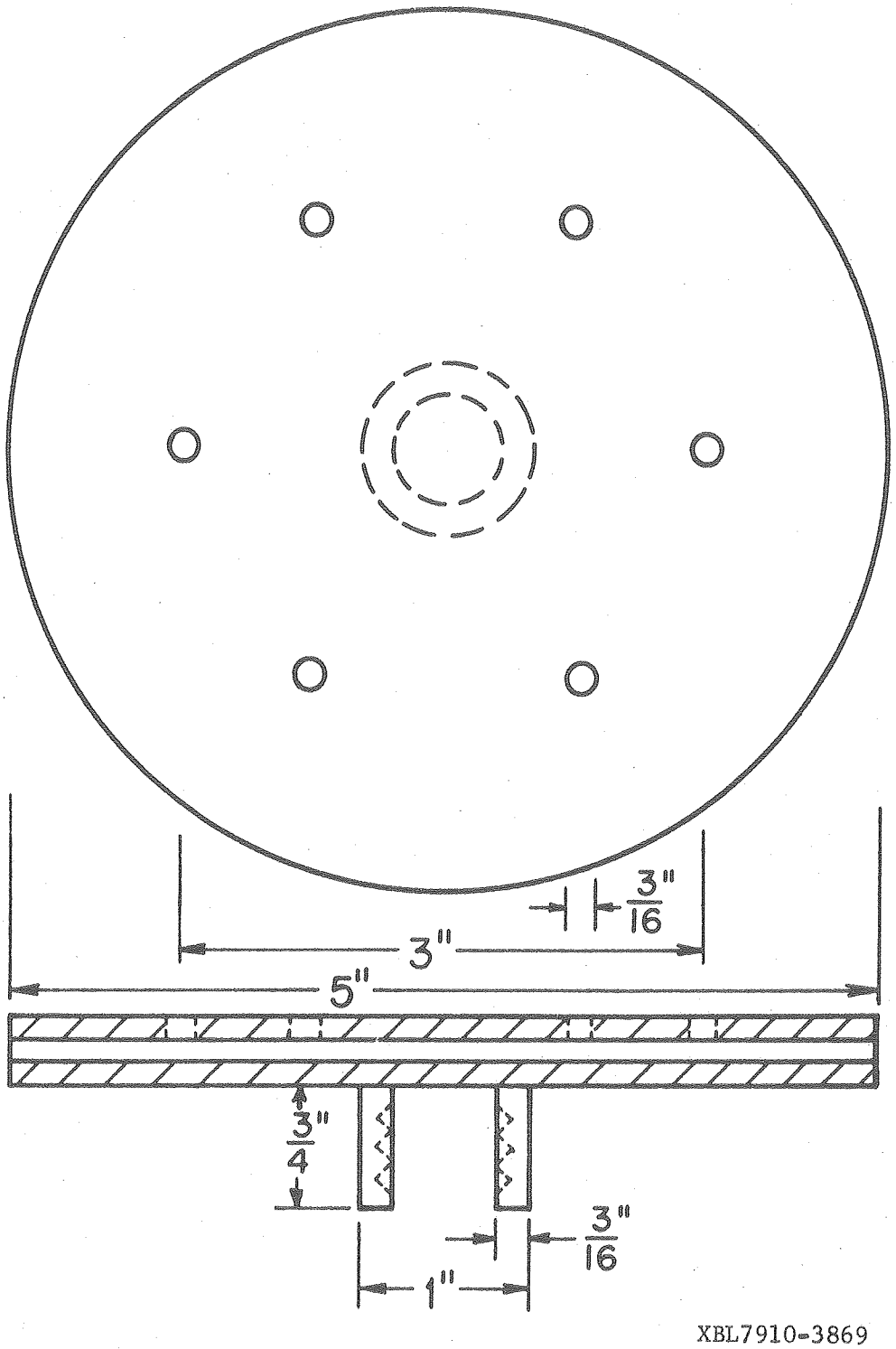

Figure III-3. Gas Sparger (6-5mm Orifices)

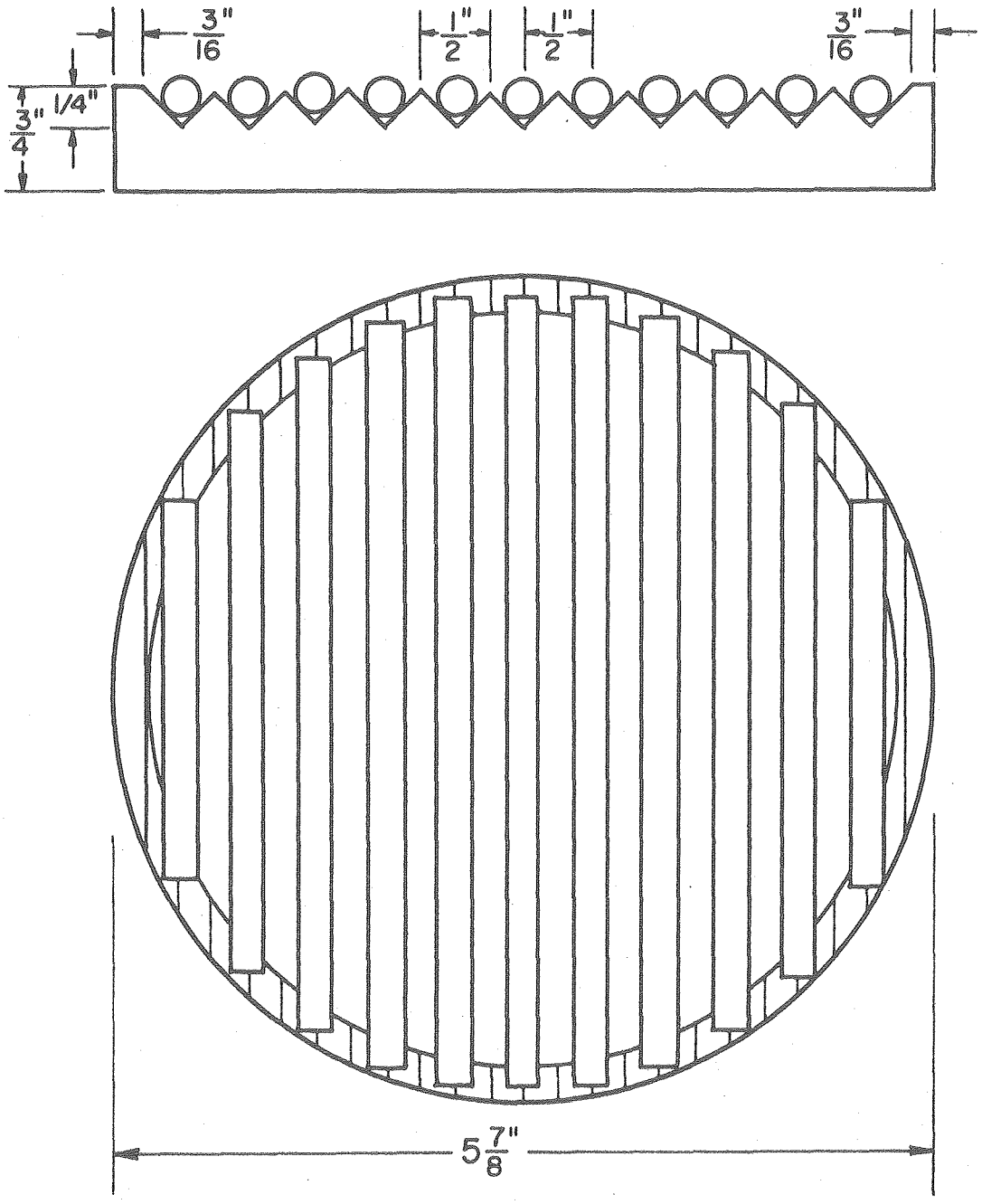

Figure III-4. 1/4-inch rod tray.

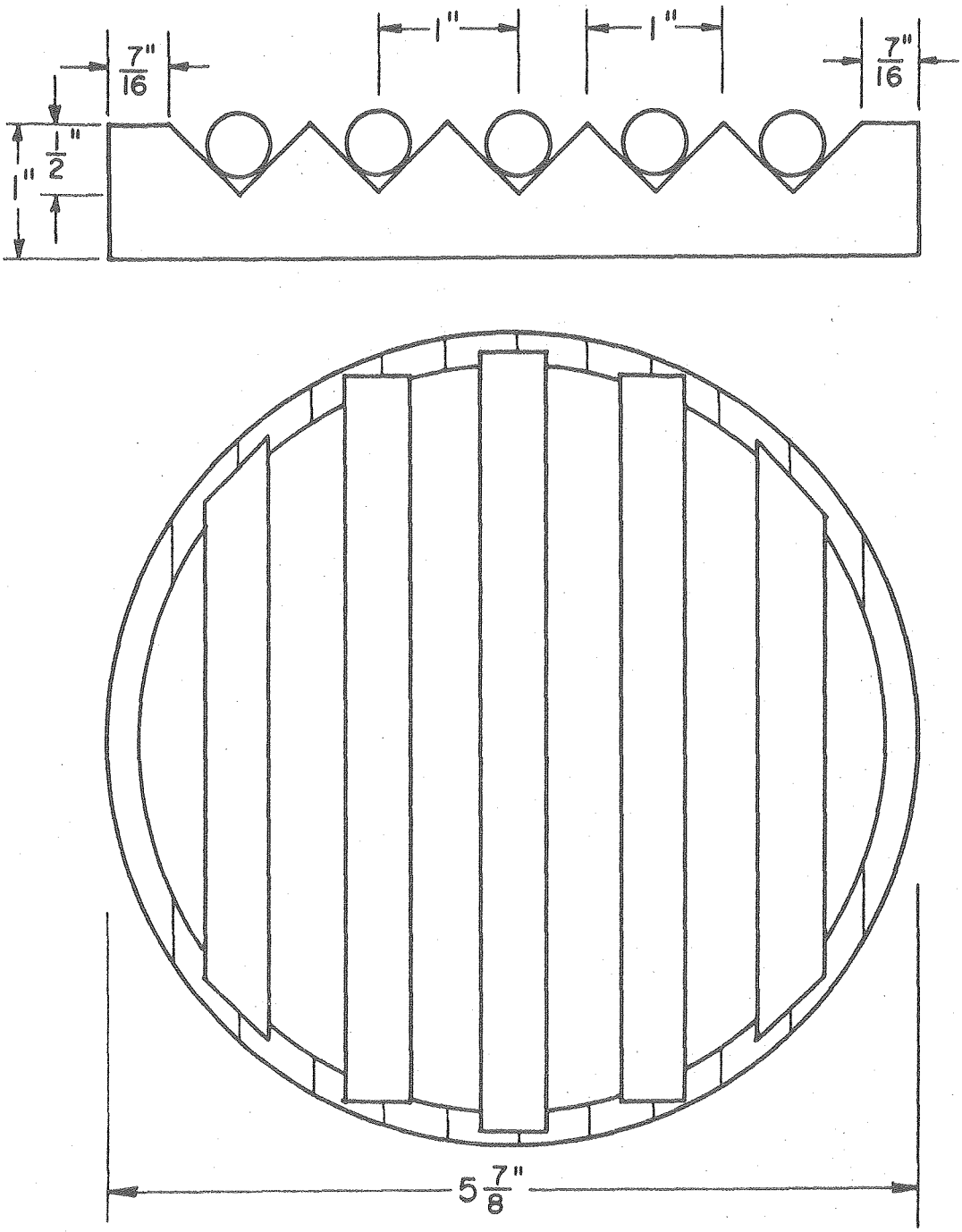

Figure III-5. 1/2-inch rod tray.

B. Helium Transient Response Apparatus

Figure III-6 depicts the equipment flowsheet used to obtain mass-transfer coefficients for desorption of helium from water and the two model liquids.

The liquid under investigation was saturated with helium for one-half hour at a gas flowrate of 0.441 ft^3/min and atmospheric pressure. The transfer lines through to the sample loop also held pure helium at one atmosphere of pressure. Before the start of an experiment the feed lines were competely purged of helium by nitrogen, using a valve arrangement designed for this purpose. This also eliminated any dead volume helium that might seep back into the nitrogen feed stream. At the start of an experiment, a stopwatch was started and zero time was recorded on the strip chart. A sample stream was sent through traps to remove impurities. A plastic tube 3/4-inch in inside diameter and 6 inches long filled with Drierite between glass wool plugs was used for the water vapor trap. To trap impurities from the model liquids, a plastic tube 3/4-inch in inside diameter and 10 inches long, half full of Drierite (upstream) and half with crushed 4Å and 13Å molecular sieves that had been heated previously to 450°C for 4 hours in an oven and cooled in a vacuum dessicator. Knowing the sample flow rate and dead volume downstream from the column permits calculation of a lag time that must be subtracted from the zero time recorded on the strip chart in order to get the true start of an experiment.

Gas flows continuously through the sample loop and is periodically injected into the thermal conductivity cell (about every 15 sec in a 5 minute experiment) by de-energizing a solenoid valve. The empty

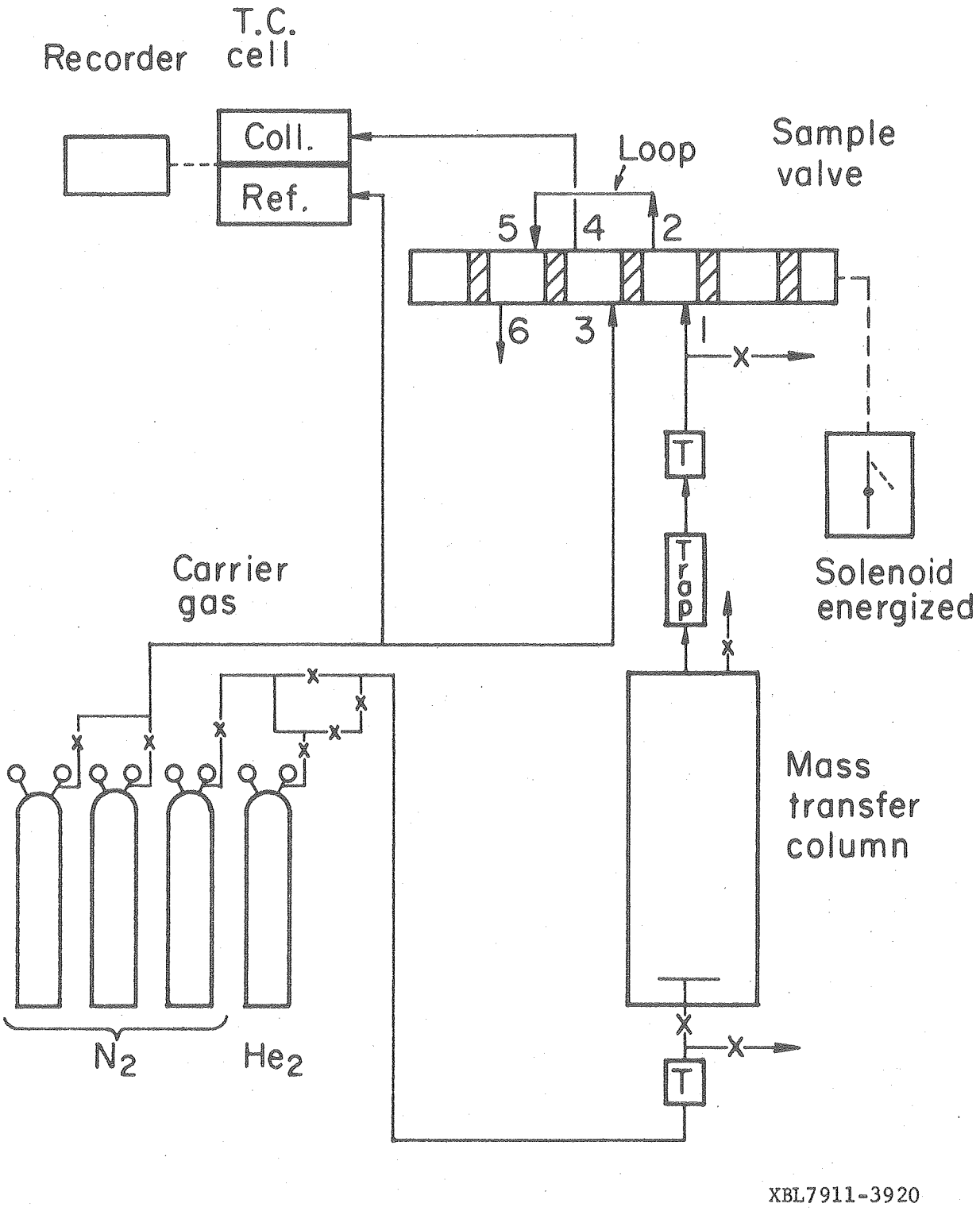

Figure III-6. Helium transient response apparatus.

1/8-inch column (about 1 ft long) downstream from the sample loop delivered a sample in about 4 seconds. After a peak had come out and been recorded on a stripchart Model 385 by Linear Co., the solenoid would be energized so that the sample loop could be filled again. The collector and reference cell flowrates were 58 and 42 cc/min., respectively. The thermal-conductivity cell was operated at 100^{o}F, to dampen the effect of room temperature changes. The strip chart was operated at 0.1 cm/s for most of the experiments.

The effect of gas velocity in the orifice, as well as orifice size, was investigated by the sparger designs shown in Figures III-7 and III-8. In the interests of brevity two other spargers of orifice diameter 1 mm are not shown. They resemble Figure III-8 except for orifice size and spacing. One had a centered orifice; the other had two additional orifices, one being a 3-inch bolt circle.

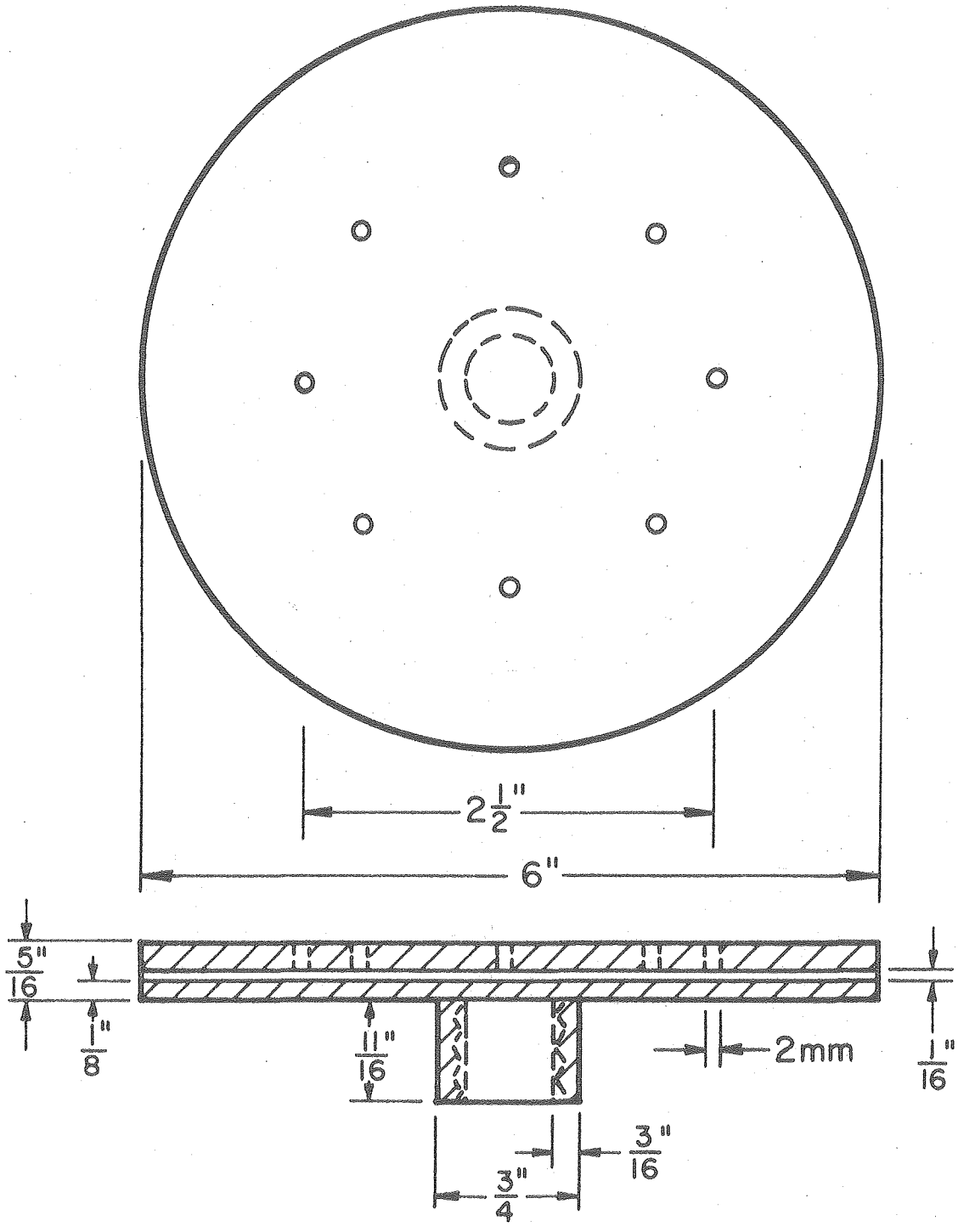

Figure III-7. Gas sparger (8-2 mm orifices).

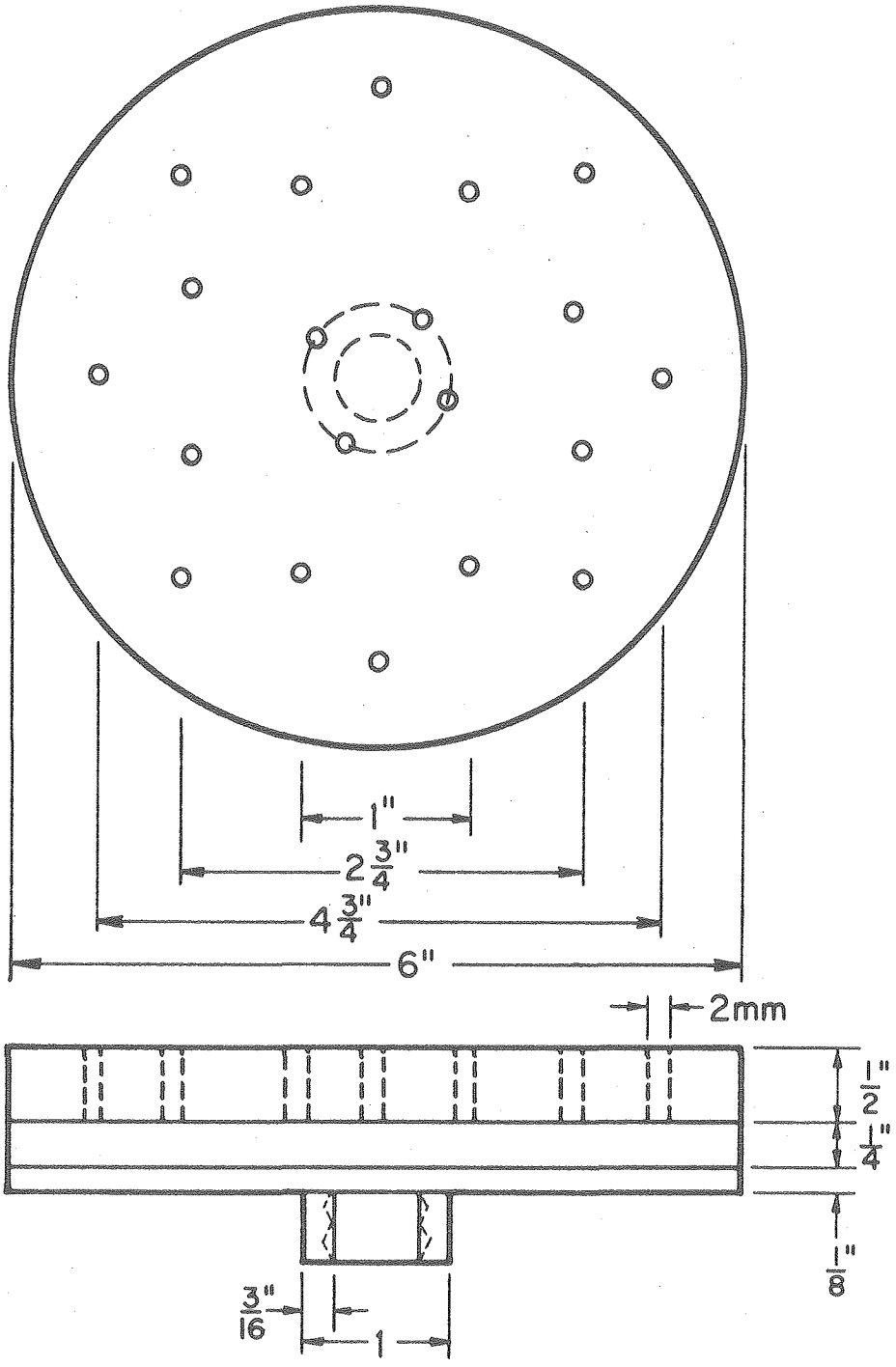

XBL7911-3923

Figure III-8. Gas sparger (20-2 mm orifices).

IV. Coal Liquefaction Reactor Design

A. $ZnCl_2$/MeOH Coal Liquefaction Reactor Material Balances

1. Hydrogen and Coal

If the coal-liquefaction is sparged only at the bottom, this may lead to a large throughput and large holdup will occur near the bottom, while a hydrogen deficient operation may still arise near the top due to hydrogen consumption. Coalescence of the remaining gas bubbles, into very large fast rising or small bubble entrainments in the downward flowing melt may lead to unwanted char formation in the upper hydrogen-deficient zone.

Such imbalance of hydrogen flow can be avoided by multiple feeding of hydrogen at discrete levels along the reactor length, uniformly over each cross-section. The basis for the amount of hydrogen fed to each section, in this case is

1. A certain percent of coal conversion (up to 25%) occurs within each section.
2. The minimum ratio of hydrogen needed per atom of carbon converted is 1:4. Also, up to half the hydrogen consumed goes into producing water.

Much of the coal conversion (S8) occurs through the splitting of ether linkages by the reaction:

$$R\text{-}O\text{-}R + 2H_2 \rightarrow 2RH + H_2O$$

In sub-bituminous coals there is about one oxygen atom for each eight carbon atoms, and apparently up to 75% of the oxygens are ether-like (H2).

Calculations for a 1 ft^2 cross-section of coal melt column under commercial conditions can be found in Appendix F. The total hydrogen feed is taken to be about 60% in excess. One third of this excess (that is, 20% of stoichiometric) is to be fed into the coal melt prior to heat-up and entry into the reactor, so that any reaction occurring then will form the desired liquefaction products and not char.

Figure IV-1 shows a schematic diagram of the reactor with streams labeled for hydrogen, coal, and liquid and gas phase water. The latter, as a reaction product, is labeled as a separate stream for conceptual purposes only and is treated in the next section.

Table IV-1 lists the flowrates for hydrogen and coal entering, and reacting in, each section (numbered from the top), along with the superficial gas velocity entering and leaving each stage (an important hydrodynamic variable with respect to design).

It is projected that the top two reactor sections will be operated at 275°C, and the bottom three at 325°C. Compared with 250°C operation in Shinn's study, the residence time for conversion will be reduced substantially. At low conversion, coal reactivity is high due to reaction of ether linkages. At higher conversions most of the ether bonds have reacted. Higher temperatures are then needed to drive the reaction to completion.

2. Water

If the moles of oxygen reacted from ether-like bonds results in equivalent water production, an inventory of the water content in the gas and liquid phases is warranted. Above 17 wt% of methanol in the $ZnCl_2$/methanol melt the activity of the melt decreases (S8).

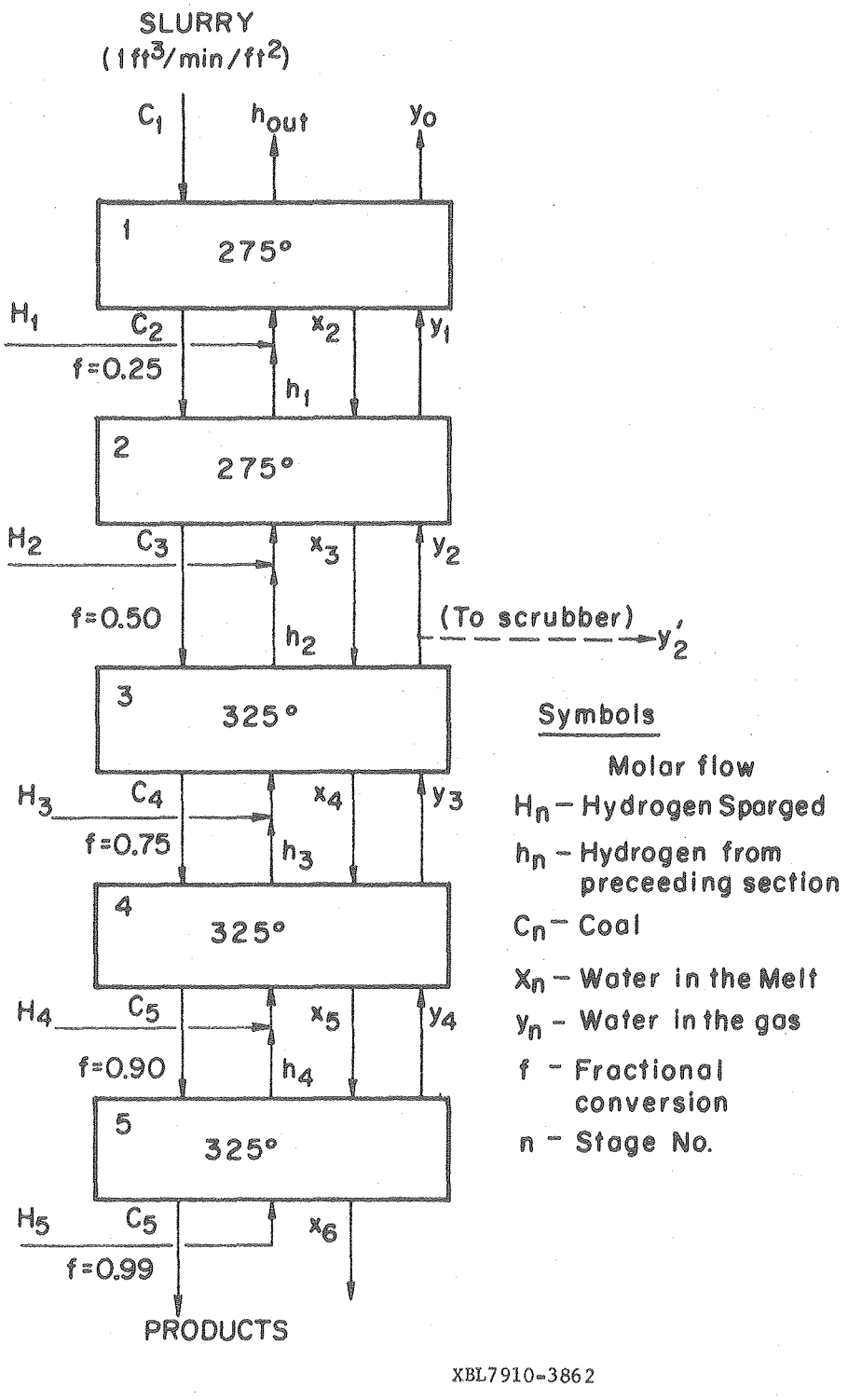

Figure IV-1. $ZnCl_2$/MeOH coal liquefaction reactor schematic diagram.

Table IV-1

Intermediate Hydrogen Flowrates, Coal Conversion and Superficial Gas Velocities

For The Conceptual Liquefaction Reactor, Basis: 1 ft^2 of Reactor Area

Stage	Coal Conversion %	H_2 Feedrate lbmoles/min	H_2 Reacting lbmoles/min	Linear Gas Velocity meters/min	
				Entering	Leaving
1	0-25	0.147	0.061	0.53	0.33
2	26-50	0.147	0.061	0.49	0.29
3	51-75	0.147	0.061	0.49	0.27
4	76-90	0.123	0.036	0.36	0.23
5	91-99	0.123	0.023	0.22	0.14

Mole for mole, water is believed to have a similar effect, so that steps may be needed for its removal.

Figure IV-1 indicates the intermediate flows of streams for water in the gas and liquid phases for two cases. If gas-phase scrubbing for water removal is desired, the gas stream labeled y_2' should be withdrawn from the top of the uppermost 325°C section. It is believed this will give optimum water removal for a single step. The high partial pressure at the higher temperature makes the gas a "sink" for water from the lower lying sections. If this water is not removed, it largely condenses into the melt in Section 2.

The partial pressure of water in any stage n can be represented by

$$P_n = f(T, W_w)$$

with P_n the water partial pressure, T the temperature, and W_w the effective weight fraction of water, as reported by Holten (H5) and shown in Figure VI-A1. The combined effect of water and of 17 wt% methanol dissolved in the melt is taken into account by assuming:

$$W_w = 0.085 + W_n$$

where W_n represents the weight fraction of water in any stage. This relation assumes that the bonding capacity of methanol and water are equal on a molar basis, and that the methanol is bound more tightly than water. The gas-phase water flowrate was then calculated from the relation

$$Y_{n-1} = \frac{P_n}{P_{tot} - P_n} F_n$$

where F_n = Average hydrogen flowrate, lbmole/min., and P_{tot} = Total reactor pressure, psi.

The calculation is iterative, starting by assuming a liquid water flowrate leaving the bottom stage, calculating P_n, Y_{n-1}, and X_n from

$$X_n = X_{n+1} + Y_{n-1} - Y_n - G_n$$

where G_n is the moles of water generated by the amount of chemical reaction occurring in the section.

Table IV-2 shows the intermediate partial pressure and water liquid weight-percent for the scrubbing and non-scrubbing cases. Scrubbing reduces the maximum water weight-percent in the melt from 6.8 to 2.3%, and also removes 77.6% of the total water formed while 84.6% remains without scrubbing. For these reasons a strong case can be made to include the scrubber in the final design.

B. Experimental Study and Data Interpretation

Experiments were performed to obtain the gas holdup and liquid mass transfer coefficients for three liquids used to model the $ZnCl_2$ catalyzed process.

1. Gas Holdup

The determination of the interfacial area, a, available for mass transfer can be obtained from the relation

Table IV-2

Intermediate Partial Pressures and Weight Fraction for Water
In Scrubbing and non-Scrubbing Systems

	With Water Scrubbing		Without Water Scrubbing	
Stage	Water Wt%	Partial Pressure psi	Water Wt%	Partial Pressure psi
1	1.54	90	1.76	90
2	1.84	90	6.68	125
3	2.18	240	5.93	330
4	0.93	240	5.22	295
5	1.12	240	4.06	275

$$a = 6\varepsilon_g/d_b \qquad (1)$$

Here d_b is the average bubble diameter (which will be discussed later), and ε_g is the holdup or volume fraction of gas in a unit volume of slurry mixture. It can be determined experimentally for an empty column from the relation

$$\varepsilon_g = (L-L_o)/L \qquad (2)$$

where L is the total liquid height and L_o is the settled height or, for a column with internals of volume I,

$$\varepsilon_g = (L-L_o)S/(LS-I)$$

where S is the superficial cross-sectional area. The main correlating parameters influencing holdup are the liquid physical properties and the superficial gas velocity U_g.

Superficial velocities and mass velocities needed for hydrogen at elevated pressure lie in the range of accessible values for air at atmospheric pressure. Figure IV-2 to IV-4 show holdup data in the 6-inch column (ranging from 0 to 20 vol.%) for tap water and for 22-cp and 84-cp zinc chloride solutions. For an open column, at all three viscosities, the orifice gives less holdup than the sparger. With the sparger, the trays with 1/4-inch spacing tend slightly to increase the holdup, while those with 1/2-inch spacing either lower it or have no effect. While in operation, the viscous liquids took on a murky appearance due to the formation of very small bubbles. Obtaining accurate froth-height

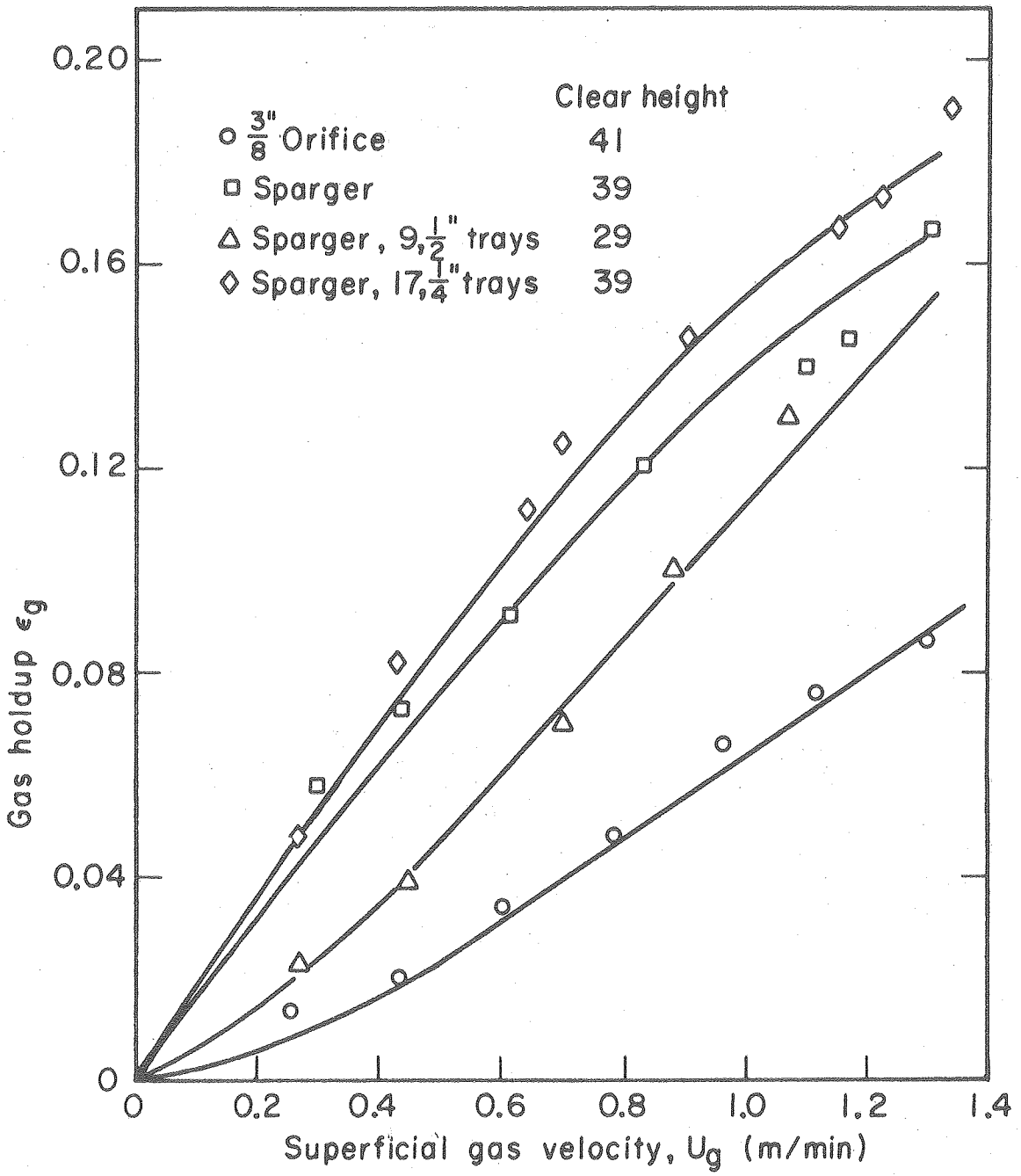

Figure IV-2. Gas holdup vs. gas velocity for tap water.

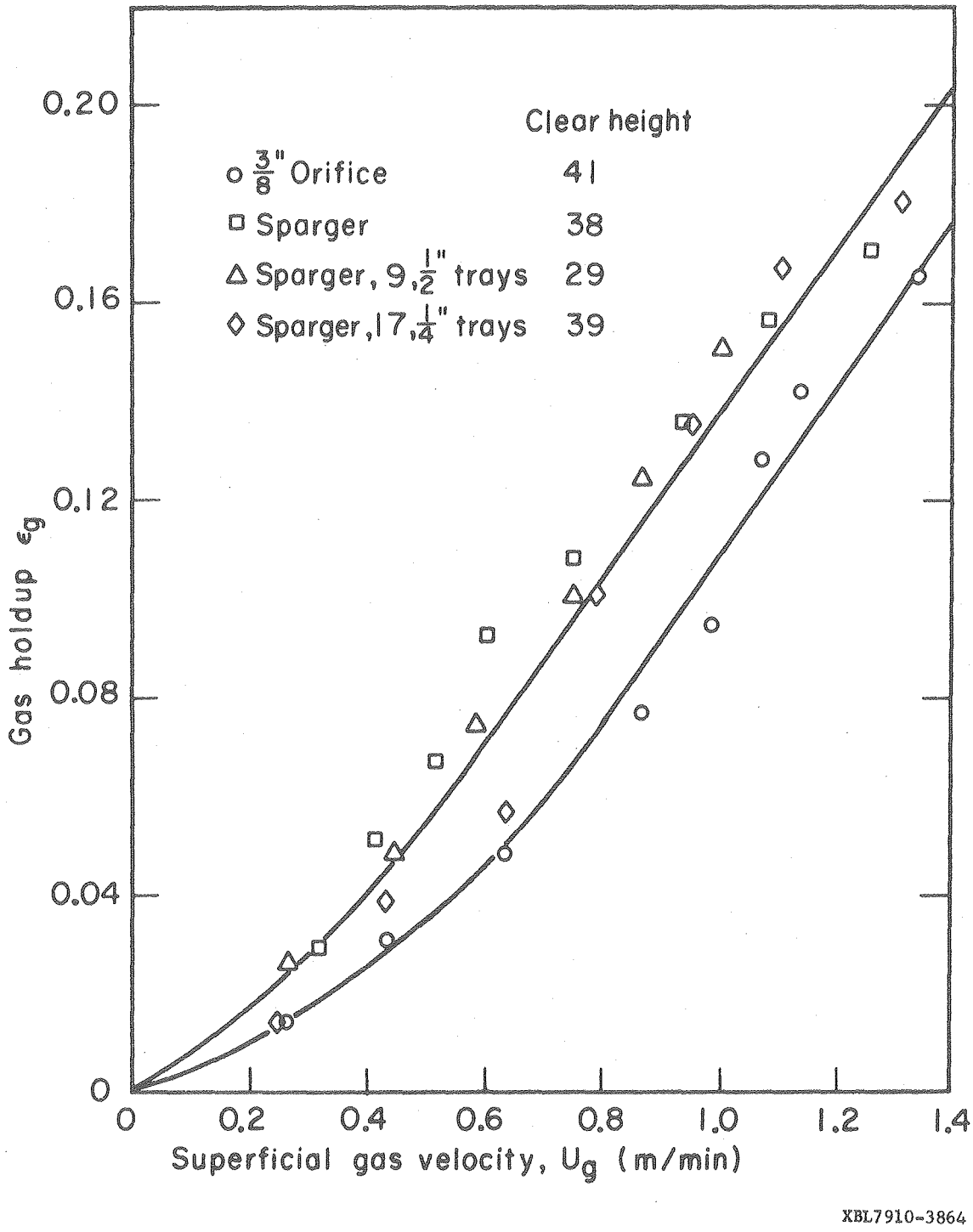

Figure IV-3. Gas holdup vs. gas velocity for 20 cp model liquid.

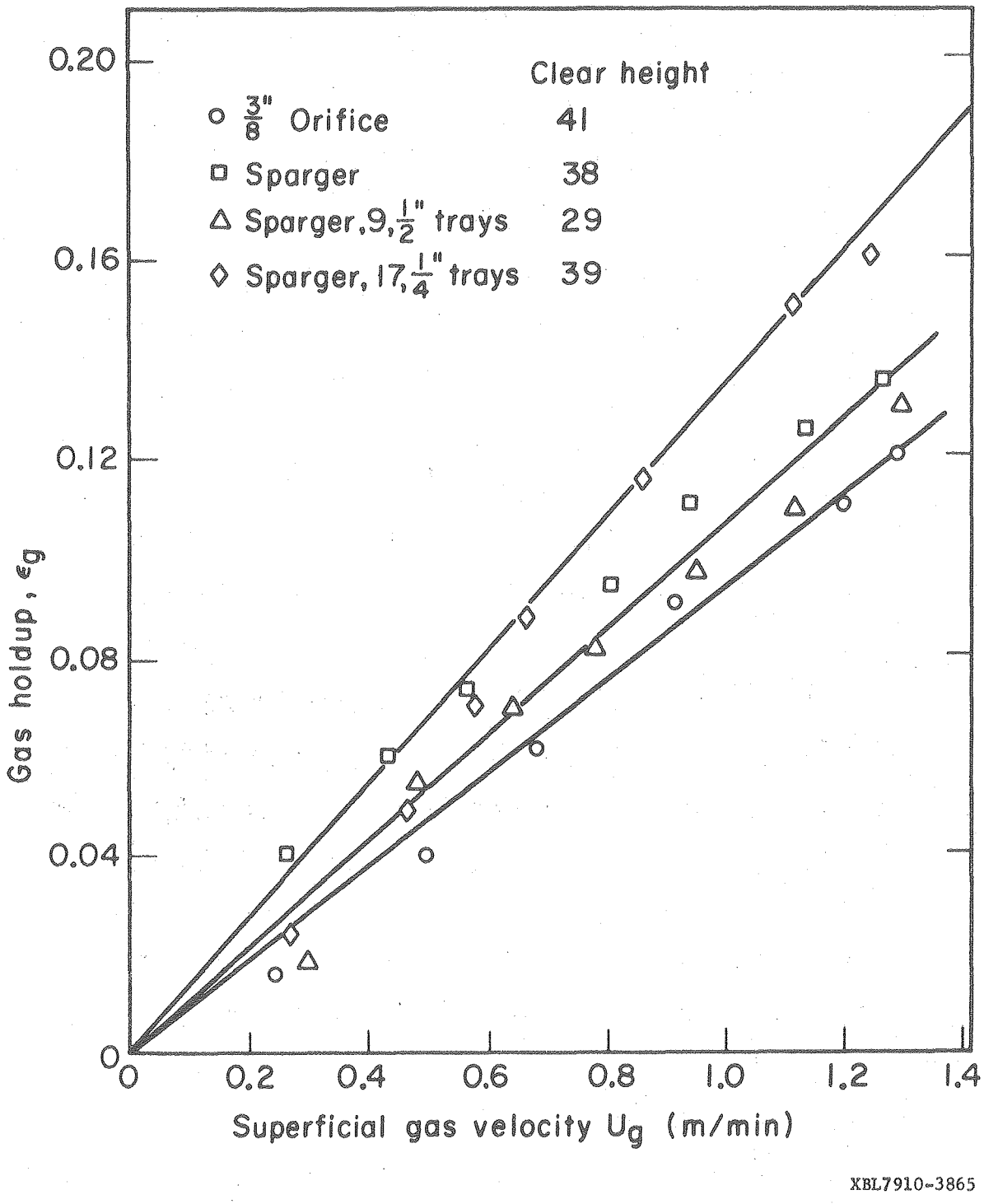

Figure IV-4. Gas holdup vs. gas velocity for 84 cp model liquids.

measurements was difficult due to a wildly fluctuating interface, the worst occurring with the orifice.

It was thought that inclusion of internals might increase the area available for mass transfer by continually breaking up the flow of gas. Except for the trays with 1/4-inch spacing, the effect of increasing viscosity is to decrease turbulence and bubble break-up and thus decrease the holdup. These observations suggest strongly that the bubble size does not change much from the sparger to the 1/4-inch trays. If it is assumed that the bubbles passing through the 1/4-inch rings are 1/4-inch in diameter, the changes in holdup in going from 1/4-inch to 1/2-inch spacing or to the open column can be used to estimate the relative bubble sizes, interfacial area per unit volume, and rates of mass transfer.

The holdups presented here assume uniformity everywhere above the plane of introduction of gas into the column. The data are not reliable enough to give an estimate of the height at which the holdup changes from a lean value (in the vicinity of the sparger) to a value that is consistent with the major portion of the column. However, the interfacial areas calculated from these holdups will be lower than the true area above the sparger, and thus will present a conservative estimate for design.

2. Liquid Mass-Transfer Coefficients

Two experimental techniques were employed in our effort to obtain mass transfer coefficients for the model liquids. The first, which proved unsuccessful, used n-propanol as a transferred component into the gas phase in a static equilibrium apparatus. It was found

that despite numerous steps to reduce the mass-transfer rate, the gas phase was always essentially in equilibrium with the liquid. A discussion of these results is given in Appendix G.

The second technique employed involved saturating the liquids with helium and measuring the transient response (V1). These experiments proved successful, and have paved the way for future two-phase and three-phase mass transfer research in bubble columns. The mathematics presented here follow the outline originally presented by Schaftlein et al. (S3) and was actually employed in a study of a three-phase stirred tank by Joosten et al. (J2).

The liquids are saturated with helium, and a step change is made to a feed of pure nitrogen. The desorption of helium with time is measured by sending pulsed samples (at 15-second intervals) to a thermal conductivity detector, using a pure nitrogen reference. The detector measures a stream of helium in nitrogen, decreasing in helium content with time, that can be used to deduce a mass-transfer coefficient.

The gas-phase helium concentration is a function of position and time. An unsteady-state material balance yields

$$\varepsilon_g v_b \frac{\partial C_g}{\partial z} - k_l a \left(C_l - \frac{C_g}{H} \right) = \varepsilon_g \frac{\partial C_g}{\partial t} \qquad (4)$$

Experimental data for water and the viscous melts show that

$$\frac{\partial C_g / \partial t}{\partial C_g / \partial (z/V_b)} \approx 0.025 \qquad (5)$$

so that the time derivative can be ignored. A physical interpretation would be that in the time it takes a bubble to rise one column length, the concentration change at the top surface is 2.5% of that bubble's soluble content.

Boundary conditions for pseudo-steady state at zero time are

$$@\ z = 0 \qquad C_g = 0$$

Integration yields

$$C_g(z) = HC_l(0)\left[1 - \exp\left(\frac{-k_l a\ Z}{v_b \epsilon_g H}\right)\right] \tag{6}$$

The liquid is considered to be well mixed, and hence the liquid concentration is a function of time only. At zero time, with atmospheric operation

$$HC_l(0) = \frac{1\ atm}{RT} = C_g^o \tag{7}$$

At any time the gas phase concentration at the liquid surface is related to the liquid concentration by

$$C_g(t,L) = HC_l(t)\left[1 - \exp(-\alpha)\right] \tag{8}$$

$$\alpha = \frac{k_l a\ L}{v_b\ \epsilon_g\ H} \tag{9}$$

An Overall Mass balance on the helium column yields

$$qC_g(t,L) = -V_l \frac{dC_l}{dt} \tag{10}$$

Substituting from equation 8, $C_l(t)$ into equation 10 yields

$$\frac{dC_g}{C_g} = \frac{-qH}{V_l}\left[1 - \exp(-\alpha)\right] dt \qquad (11)$$

The boundary condition is obtained from equation 8,

$$C_g(0,L) = C_g^0\left[1 - \exp(-\alpha)\right] \qquad (12)$$

Then integrating equation 11 with this boundary condition yields

$$\frac{C_g(t,L)}{C_g^0} = \left[1 - \exp(-\alpha)\right] \exp - \left[(1 - e^{-\alpha}) \frac{qH}{V_l} t\right] \qquad (13)$$

If one assumes that for gas-liquid columns

$$q = U_g S = \varepsilon_g v_b S \qquad (14)$$

and

$$V_l = SL \qquad (15)$$

then equation 12 becomes

$$\frac{C_g(t,L)}{C_g^0} = \left[1 - \exp(-\alpha) \exp\right] - \left[\left(\frac{1 - e^{-\alpha}}{\alpha}\right) k_l a t\right] \qquad (16)$$

The use of equation 13 for three phase systems is a point of contention (K2) because of solids entrainment in bubble wakes. Thus for a three phase system one must use equation 13.

A material balance on the dead volume above the liquid surface becomes

$$\frac{dC_r}{d(t/\tau_d)} + C_r = C_g(t,L) \qquad (17)$$

where τ_d is the dead-volume time constant (V_d/q). C_r, the helium concentration leaving the dead volume, is assumed the same as that at the detector, where it will have sustained an additional short time lag. Substituting the partial pressure P_r at the recorder for C_r and using the boundary condition that at time zero the partial pressure is 1 atm of helium, the solution of equation 17 is

$$\frac{P_r(t)}{1\ atm} = \frac{C_r(t)}{C_g^o} = \exp(-\bar{t}) + \frac{1 - e^{-\alpha}}{1 - M\tau_d} \left[\exp(-M\tau_d\bar{t}) - \exp(-\bar{t})\right] \tag{18}$$

where

$$\bar{t} = t/\tau_d \tag{19}$$

$$\tau_d = V_d/q \tag{20}$$

$$M = K_l a \left(\frac{1 - e^{-\alpha}}{\alpha}\right) \tag{21}$$

At sufficiently large $\bar{t}$, exp $(-\bar{t})$ decays effectively to zero, and equation 18 becomes

$$\frac{P_r}{1\ atm} \cong \frac{\alpha}{1 - M\tau_d} \exp\ (-M\tau_d\bar{t}) \tag{22}$$

because 1-exp(-α) for small α approaches α itself. This section of a semilog plot of P_r (or peak height based on a calibration standard) versus $\bar{t}$ will yield a straight line with a slope of $-M\tau_d$ and an intercept at zero time of $\alpha/(1-M\tau_d)$. For helium in water, the Henry's Law constant, bubble rise velocity, and $k_l a$ at these velocities are well

known, so that the intercept calculated from the decay slope by the mathematical model can be compared with the one obtained directly from experiments (which confirms the model). Due to the small value of α, the term $(1-e^{-\alpha})/\alpha$ lies between 0.99 and 1.00 and

$$M \approx k_l a \tag{23}$$

Experiments were carried out with water to calibrate the system, taking advantage of published values of the Henry's Law constant (P1), bubble rise velocity (Y2), and gas holdup mentioned earlier. Thus, matching experimental and model zero-time partial pressures can be compared, as shown in Table IV-3.

Runs 11-15 show excellent repeatability of the liquid resistance term, and the needed absence of any effect of liquid height or dead volume time constant. The agreement between the experimental and model partial pressures of helium at zero time gives only qualitative confirmation of the model. When they agree closely (as in runs 11, 13 and 31), the published value of the Henry's Law constant of 91.3 is well below the value calculated by the relations

$$C_l = \frac{n}{V_l} \tag{23}$$

$$n = \frac{\int_0^t n(t)dt}{t} \tag{24}$$

$$n(t) = \frac{P_r(t)\ V_t}{RT}\ ;\quad V_t = q \times \text{(Time of experiment)}$$

Table IV-3

Mass-Transfer Coefficients and Experimental/Model Intercepts

for Helium Desorption from Water

Run No.	U_g met/min.	L	τ_d	ε_g	Zero-Time Intercept Atm.		$k_l a$, s-1	Henry's Law Constant, H	Sparger Holes/Diameter
					Exp.	Model		cm^3gas/cm^3 liquid	
11	0.571	44	14.7	0.074	0.0069	0.0072	0.022	121	6-5mm
12	0.657	25	30.6	0.083	0.0068	0.0106	0.023	77	6-5mm
13	0.657	35	20.1	0.083	0.0060	0.0064	0.020	104	6-5mm
14	0.657	49	6.8	0.083	0.0094	0.0071	0.023	149	6-5mm
15	0.657	25	30.1	0.083	0.0072	0.0102	0.023	81	6-5mm
29	0.294	50	15.6	0.035	0.0113	0.0051	0.0087	*	8-2mm
30	0.536	50	8.5	0.056	0.0094	0.0074	0.0183	*	8-2mm
31	0.0727	48	6.3	0.085	0.0105	0.0102	0.329	132	8-2mm
32	0.882	48	6.9	0.095	0.0083	0.0135	0.043	235	8-2mm

*Not available

In runs 12 and 15, the literature value is above the experimentally estimated value. Since runs 12 and 15 were made with a low liquid level, it is possible that the solution was not fully saturated with helium in all the other runs. Such a starting condition has no effect on k_{1a}.

Figure IV-5 shows k_1a for water, plotted as a function of superficial gas velocity U_g for the data of Table IV-3. Data are plotted for 20 wt% $ZnCl_2$ in water which show no real difference from pure water. There is good agreement between these data and those of Akita and Yoshida (A1) that are plotted on the same figure. They measured k_1a by absorbing oxygen with sulfite oxidation at 30°C in a 6-inch column. If one makes the standard assumption of a one half power dependence of k_1a on diffusivity then the values of k_1a for oxygen can be increased by 73% in order to be compared with helium. When this is done the two lines are in good agreement and any errors can be explained by the difference in the analytic methods from which k_1a is obtained.

Obtaining mass transfer data for the viscous liquids proved difficult. This was due to the difficulty in trapping out impurities from technical grade glycerol or $ZnCl_2$ that interfered with the helium peak at the detector. Mass spectrometer analysis showed the presence of chlorine (MW=71) and a hydrocarbon peak (MW=44) presumably propane as well as CH_3^+ radicals which lends credence to the propane possibility. Traps consisting of dry ice in acetone and liquid nitrogen failed to remove them. However, a trap filled with mixed 4 Å and 13 Å crushed molecular sieves, prepared by treating at 450°C for four hours, gave a fair but imperfect removal. The resulting scatter in the plots

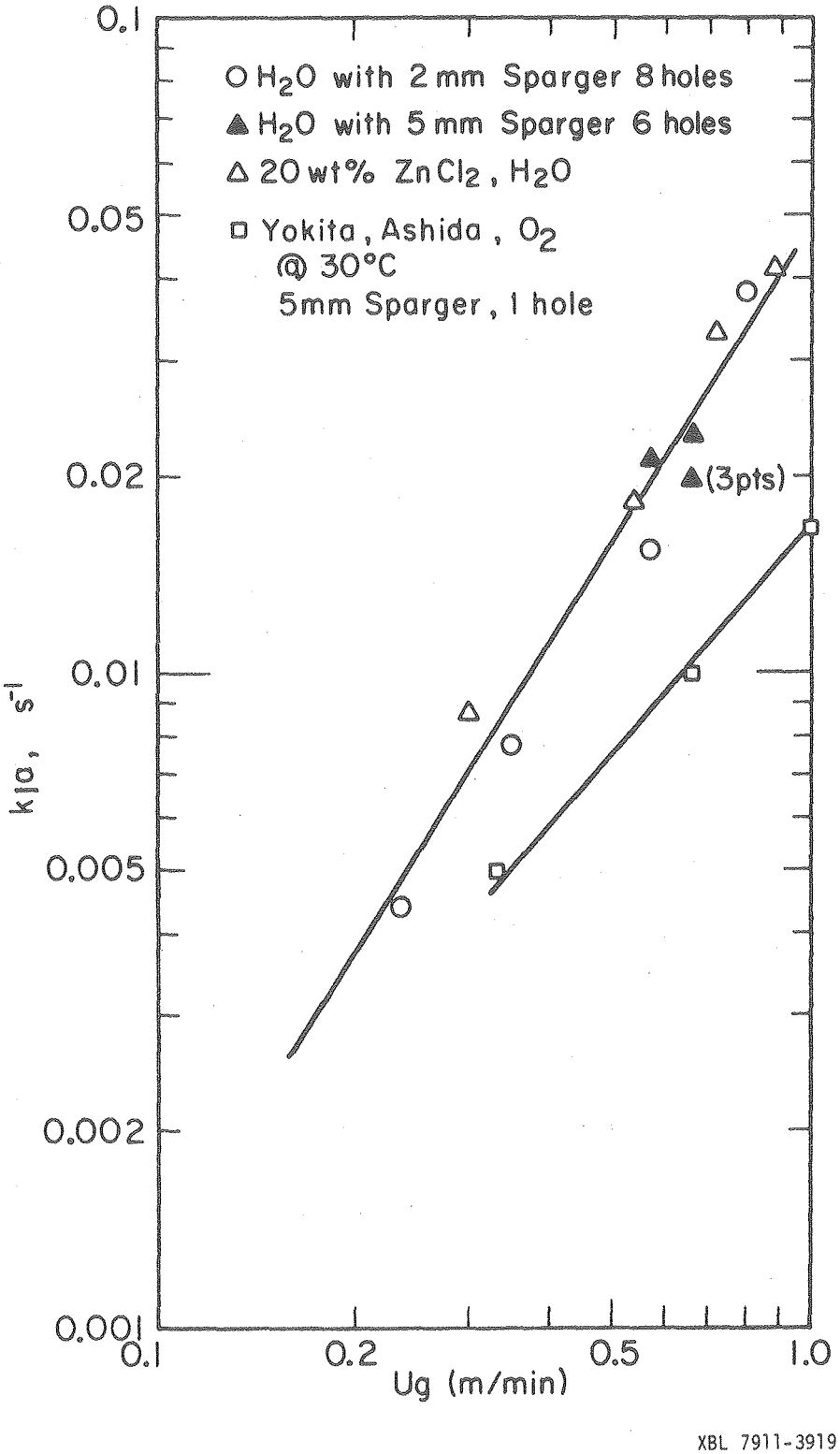

Figure IV-5. k_1a vs. gas velocity for helium desorption from water, 20 wt% $ZnCl_2$ in water, Yokita and Ashida's Data for sulfite oxidation.

of partial pressure vs. time constant, from which each $k_l a$ value is obtained, carries through the ensuring plots. Obtaining $k_l a$ from water data proved easy in comparison, due to the complete removal of water by drierite. Figure IV-6 shows mass-transfer data for the model liquids. The data show that the effect of the 1/4-inch rod trays is negligible which is consistent with the holdup data. The effect of viscosity on $k_l a$ is a -0.50 power dependence for the 20 cp liquid and a -0.55 power for 84 cp liquid. These results can be discussed with respect to other researchers correlations in order to establish the effect of $ZnCl_2$.

The effect of viscosity on holdup at these low gas flowrates has been shown to be negligible for the 20 cp liquid and to have a slight effect on the 84 cp liquid. Since viscosity is known to have an effect on the terminal rise velocity of gas bubbles a value of -0.05 power was chosen for the effect and hence a +0.05 power dependence was chosen for gas holdup. Hiss et al (H4) report that diffusivity varies with viscosity to the 0.67 power while the dependence of bubble size on viscosity has been shown to be to the 0.1 power (B3). With these assumptions the effect of $k_l a$ can be shown for other researchers correlations as well as the present work. This is shown in Table IV-4.

These results show that the effect of $ZnCl_2$ in a viscous medium is well within that reported in the literature for viscous liquids alone. This is also consistent with the mass-transfer data for 20 wt% $ZnCl_2$ in pure water where it was shown that the $ZnCl_2$ had no effect. This does not, however, show the effect of surface tension which could be much lower than that of the model liquids (64 to 77 dynes cm).

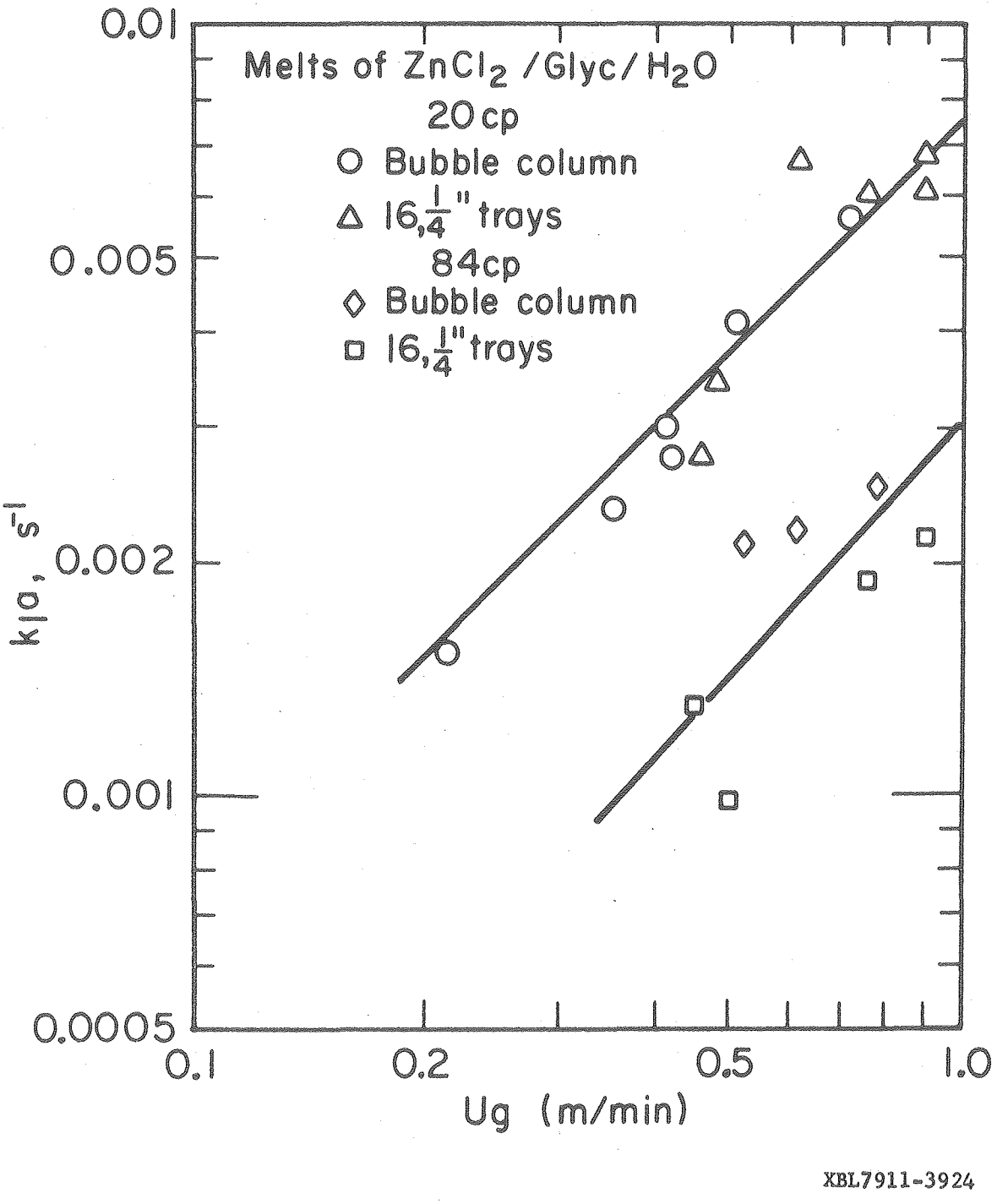

Figure IV-6. k_1a vs. gas velocity for model liquids in bubble column and with 1/4-inch rod trays.

Table IV-4

Comparison with other Researchers' Correlations for the Effect of Viscosity on Liquid-Side Mass-Transfer Coefficients, $k_l a$

Investigator	$k_l a$ Power Dependence on Viscosity
Calderbank	-0.55
Hughmark	-0.50
Higbie	-0.48
Akita	-0.43
Present Work	-0.50

Figure IV-7 shows the effect of the number of orifices and orifice diameter on $k_l a$ in helium desorption from water. At a constant superficial gas velocity a single orifice sparger with a diameter of 1mm increases $k_l a$ by 25% over a 3 orifice sparger with the same diameter. A gas jet was observed at the 1-1mm orifice that is considered to be the cause of the increased mass transfer rates. The dashed line in the figure is the same solid line used in Figure IV-5 where the other water data is plotted. Thus these results show that by adding orifices of 1mm diameter or increasing the diameter to 2mm (or 5mm in the case of Yokita and Ashida) will have no effect on the mass-transfer coefficients.

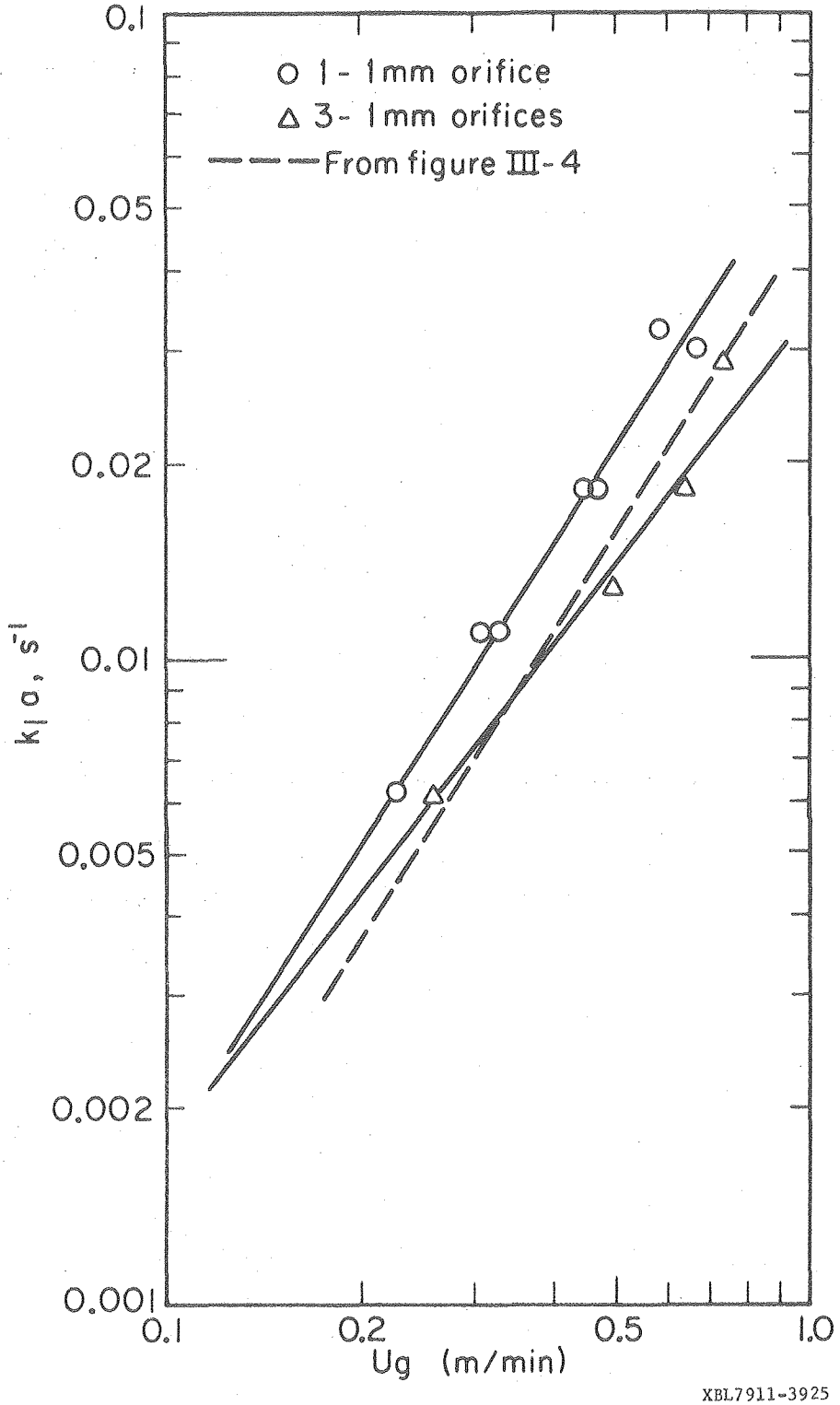

Figure IV-7. $k_l a$ vs. gas velocity for 1mm orifice and 3-1mm orifices for helium desorption from water.

V. Conclusions and Recommendations

1. The absorption of hydrogen in a three-phase coal liquefaction reaction can be represented by a resistance-in-series model.
2. Repeatable mass-transfer data for two-phase and three-phase systems can be obtained using a transient-response method. This method, with refinements, could be applied directly to a coal liquefaction reactor to yield quantitative mass-transfer coefficients and semi-quantitative Henry's Law constants.
3. Static equilibrium experiments, using a highly soluble liquid (n-propanol) as a transferred component, result in gas saturation and thus cannot be used to obtain mass-transfer coefficients in the apparatus depicted in Figure III-1.
4. The effect of rod-tray internals with respect to mass-transfer and gas holdup is negligible (which does not invalidate their use).
5. The effect of $ZnCl_2$ in water and in a viscous medium (glycerol) is negligible with respect to mass-transfer and gas holdup for liquids with surface tensions in the vicinity of that for water.
6. Water build-up in the gas phase of the reactor should be compensated for by diverting the gas to a water scrubber system partway through the reactor, in order to keep the catalytic activity of the $ZnCl_2$/MeOH melt at a maximum.
7. It is assumed that the effects of small particles and much lower surface tensions in the reactor will decrease the mass-transfer rate by no more than one order of magnitude. However, even this much reduction will only represent 25% of the projected overall

absorption rate. Thus, for practical purposes, the chemical reaction rate can be assumed to be controlling.

8. Finally, the notion that a slurry reactor can be fundamentally understood by filling in "holes" in the literature is summarily rejected. To achieve usable results, comprehensive study of the system variables is needed.

It is recommended that:

1. Experimental and theoretical reactor research for slurry reactors in general and coal liquefaction reactors in particular should start from a gas-liquid bubble column, and using existing knowledge as a guide, build up in complexity in order to understand the interactions of design variables.
2. The transient response system should be improved (i.e. by continuous gas sampling) to ensure that the zero-time intercept and Henry's Law constants (which poorly agree with published values) are correct.
3. The effects of low surface tension and particle size (10 to 100 microns) should be studied in bubble columns, and these results integrated into the general development.
4. Rod trays should be retained in the reaction design, although they have no effect with respect to mass transfer and gas hold up, because they serve to keep the slurry in plug flow.
5. A better viscous medium should be chosen or a better gas-sample stream developed, in order to eliminate the organic-chemical impurities in obtaining mass-transfer data for $ZnCl_2$ melts.

6. More work should be done in determining the gas and liquid/slurry compositions as a function of reaction coordinate for the $ZnCl_2$/MeOH system.
7. Experiments should be undertaken to determine the coal particle size as a result of breakup for the $ZnCl_2$/MeOH system.
8. Experiments should be run with the transient response method and the sulfite oxidation (or other) technique simultaneously, in order to bring into focus any regimes where the two measuring techniques disagree.

VI APPENDIX

Appendix A

Melt Viscosity vs. Temperature

Continuous measurements of melt viscosity vs. temperature over the range of 35^{o} to $112^{o}C$ were taken employing a Brookfield Model LVT viscometer and a mercury bulb thermometer, with a 83 wt% melt of $ZnCl_2$ in $ZnCl_2$/MeOH in a 1 lit. beaker open to the atmoshere and heated on a hot plate. The vapor pressure of methanol, assumed to be 5 psi, at $110^{o}C$ by analogy to water (Fig. VI-A1), is so low that allowing it to vaporize during experimentation should not cause the melt to concentrate in $ZnCl_2$ to any appreciable degree.

The Arrhenius-type behavior of melt viscosity vs. temperature in the form

$$\mu = B \exp(-\Delta E/RT)$$

is shown in Figure VI-A2 and gives an activation energy of 11.4 kcal/gmole. Extrapolation yields melt viscosity of 0.6 cp at $275^{o}C$.

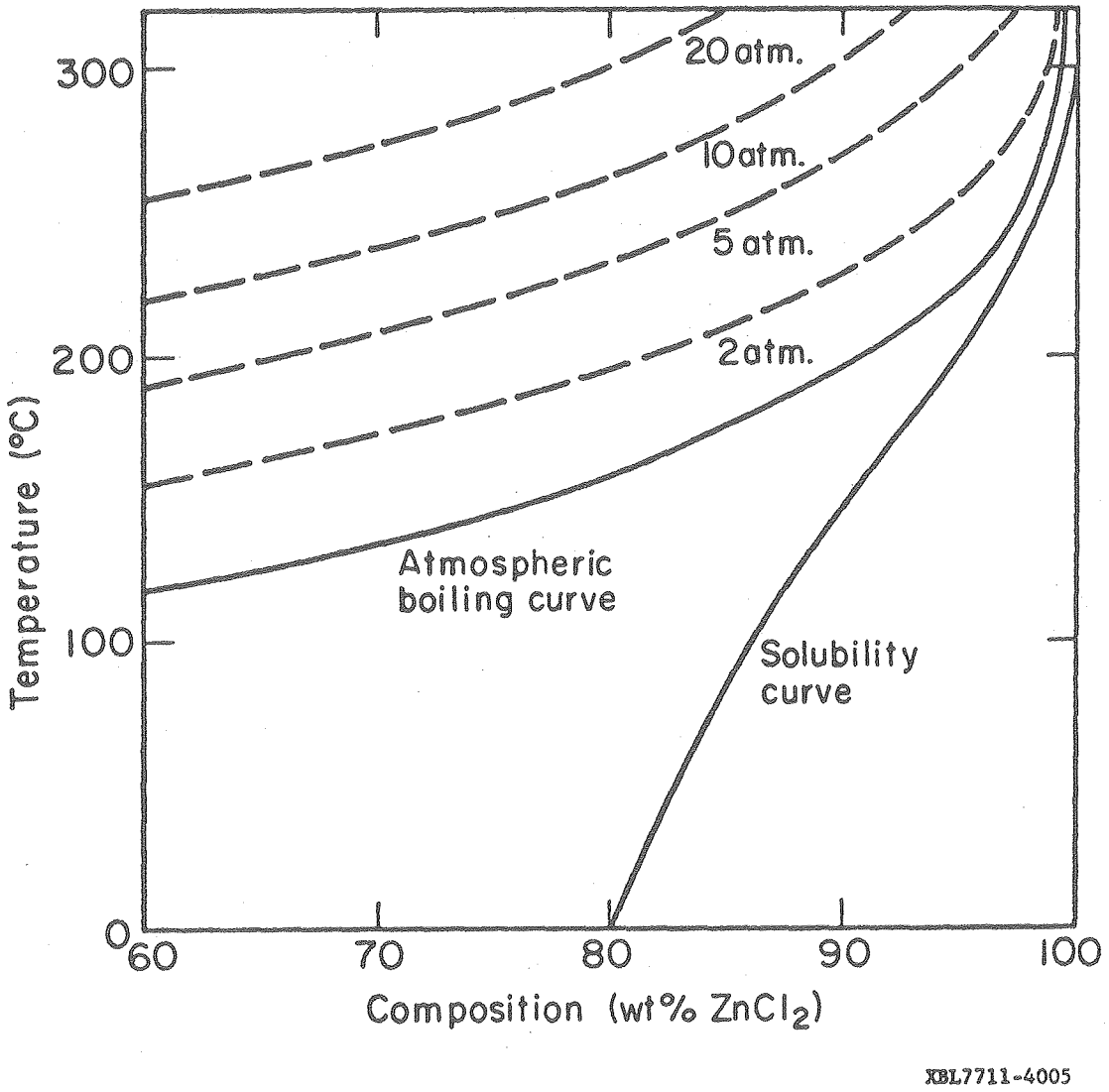

Figure VI-A1. Vapor pressure of H_2O over $ZnCl_2/H_2O$ melts.

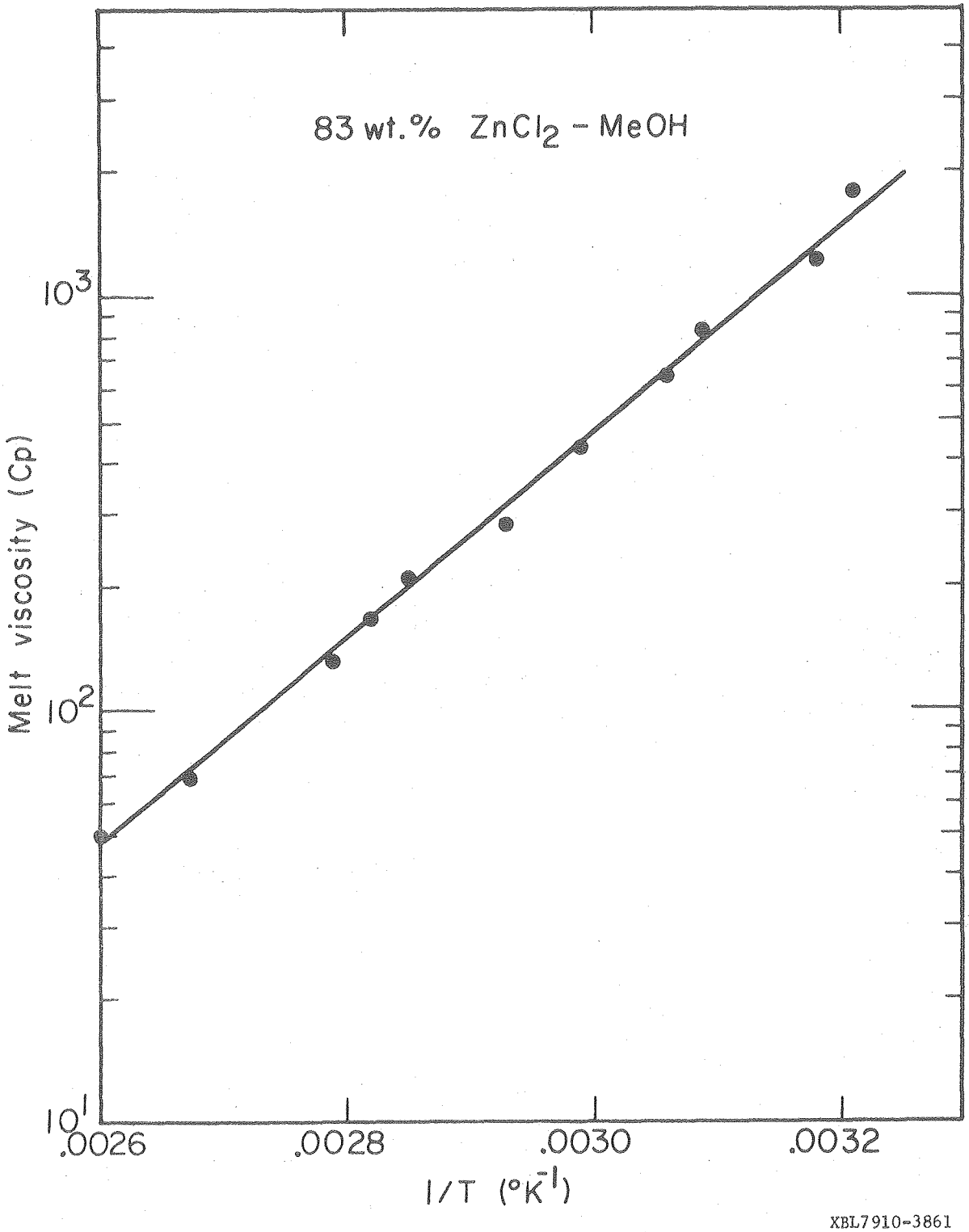

Figure VI-A2. Viscosity of 83 wt% $ZnCl_2$MeOH vs. Temperature.

Appendix B

Criteria for Series Resistance in the Absorption Rate of Hydrogen

In the three-phase reacting systems discussed in the literature, two phenomena must be addressed with respect to rate expressions for the reacting species: the solid dissolution rate, and the particle size in relation to the concentration boundary layer of gaseous reactant around the gas bubbles. The solid dissolution rate refers to the process whereby a solid species enters the liquid phase to react with dissolved gas. In the coal liquefaction process discussed here, it is assumed that no reactive coal species survive above the surface of the coal, so that the rate can be expressed in terms of a surface concentration of hydrogen. The concentration boundary layer, identified also as the liquid film thickness, represents that distance in which the concentration of gas at the gas-bubble surface decreases to that of the bulk liquid

$$\delta = D/k_l$$

Ramachandran (R1) states that for solids in the liquid film to be important,

$$dp \leq 0.1\delta$$

where d_p is the particle diameter.

The presence of solids has the effect of decreasing the hydrogen back pressure in the bulk liquid and increasing the liquid mass-transfer coefficient k_l. Table VI-B1 lists k_l, calculated from various authors' correlations at the conditions that are likely to be encountered.

Table VI-B1

Gas-Liquid Mass-Transfer Coefficients For Hydrogen In $ZnCl_2$/MeOH at 275°C, 600 psi, U_g = 1 meter/min.

Author, Reference	k_l, cm/s
Akita (A1)	2.2×10^{-2}
Higbie (H2)	2.3×10^{-3}
Calderbank (C1)	4.9×10^{-2}
Hughmark* (H5)	1.93×10^{-3}

*Considered to be erroneously low

An estimate of hydrogen diffusivity can be made from the data of Gubbins et al. (G5), who measured the diffusivity of hydrogen in KCl, $MgCl_2$, an $MgSO_4$ solutions as a function of temperature and concentration. Assuming $ZnCl_2$ can be modeled from $MgCl_2$ and that the activation energy obtained at 45°C can be extrapolated to 275°C, independent of concentration, the diffusivity of hydrogen in the melt is 4.7×10^{-5} cm/s. From this with the smallest believable value of k_l (Akita's or Higbie's), the film thickness becomes 2.1×10^{-3} cm. An order-of-magnitude error in diffusivity would only increase the film thickness to 6.72 x 10-3 cm. through a 0.5 power dependence of k_l on diffusivity. Coal particles are known to break up in a liquefaction reaction, and could decrease in size an order of magnitude to 5 microns. At a gas hold up 0.15, the actual volume of slurry in the film is 0.3% of the total (1 cm. bubble diameter). Thus, while the criteria for significant enhancement of mass transfer in the gas film could be met (with a severe error in diffusivity), its effect on the rate of absorption is negligible, and the assumption of no reaction in the liquid film is valid.

Appendix C

Hydrogen Solubility

The only published correlation for the solubility of noble gases in molten salts, which also provide a model for hydrogen was obtained from Watson et al. (W1). They equate the free energy of solution of the gas to the free energy of formation of holes which were assumed to be of the same size as the gas molecules. The free energy obtained would apply for a continuous fluid having the same surface tension (σ) as the solvent. Correcting for changes in surface tension, they obtain an expression for the distribution between the gas and dissolved phase:

$$\frac{C_l}{C_g} = \exp\left(\frac{18.08 r^2 \sigma}{RT}\right) = \frac{1}{H}$$

where r represents the atomic radius of hydrogen.

Table IV C1 compares Henry's Law constants for Hydrogen in different systems from various investigators for possible coal liquefaction conditions as well as for helium and hydrogen in water. At these pressures

$$H' \cong RT\ \tilde{v}\ H$$

Table VI-C1 shows that an estimate of Henry's Law constant, good to within 25% can be obtained from this information. These values are not far removed from the solubility of hydrogen in organic solvents.

Table VI-C1

Henry's Law Constants for Hydrogen in Different Systems Compared to Helium in Water

System	H' (Atm/Mole Fraction)	Reference
268°C, Hydrogen-Tetralin	1,173	S10
200°C, Hydrogen-Benzene	1,130	B2
5°C, Hydrogen-n Hexane	1,195	B2
275°C, Hydrogen-Molten Salt (Surface Tension = 75 dynes/cm)	2,104	W1
Ibid, Surface Tension = 40 (dynes/cm)	2,104	W1
25°C, Hydrogen in Water	1,070	P1
25°C, Helium in Water	12,500	P1

Appendix D

Liquid-Solid Mass Transfer

Satterfield (S2) recommends Brian's et al. (B3) correlation for liquid-solid mass transfer to small particles in a slurry:

$$\frac{k_s^* d_p}{D} (4.0 + 1.21\ NPe^*)^{1/2}$$

where k_s^* represents a liquid-solid mass transfer coefficient calculated at the terminal settling velocity of the particle, and N_{Pe}^* is the Peclet number calculated for these conditions. The true coefficient is higher and empirically Brian found

$$k_s/k_s^* = 2$$

Hughmark (H7) presents the data of many investigators in the form of six correlations, each of which conforms to a specific regime of Reynolds and Schmidt numbers. His Reynolds number contains the slip velocity, or terminal settling velocity.

Although the closest correlation is in a regime lower than ours because liquid-liquid diffusivity is higher than gas-liquid diffusivity, the calculations of the liquid-solid resistance for these researchers show good agreement for 0.2 mm and 1.0 mm particles. These results are shown in Table VI D1. The liquid-solid resistance term is $k_s a_p$ where $a_p = \frac{6m}{\rho d_p}$.

Other correlations, not presented, are based on an assumed average power input per unit volume of slurry in an agitated tank. Applying

Table VI-D1

Liquid-Solid Mass Transfer Coefficients for Hydrogen to 1 mm and 200 μ particles

Particle Size	k_s cm/s	$k_s a_p$ s-1	Reference
1 mm	5.2×10^{-3}	0.14	B3
200 μ	1.3×10^{-3}	0.17	
1 mm	7.9×10^{-3}	0.21	H7
200 μ	2.9×10^{-3}	0.38	

this principle to a bubble column is not warranted due to dissimilar geometries.

Appendix E

Chemical Rate Constant

Figure VI E1 shows pressure-time data from Shinn (run 72) made at 800 psi and 250°C. If it is assumed that the coal liquefaction reaction is first order in hydrogen and first order in unreacted carbon then a rate expression can be written for the disappearance of hydrogen with time,

$$\frac{dC_{H2}}{dt} = k' C_{H_2} C_{carbon}$$

By assuming a consumption ratio of 4:1 for carbon to hydrogen as discussed earlier and knowledge of the Henry's Law constant (1.173 atm/mole fraction (S10)) allows for evaluation k'.

If water from the breaking of ether bonds enters the gas phase then it will affect the total pressure. Two k's were calculated assuming either all or none of the water influenced the pressure reading. These values are in pressure units 9.24 x 10-5 (atm-min)-1 and 3.05 x 05 x 10-5 (atm-min)-1, the latter being for no water influence. It was also assumed that the 210 lbs. of pressure rise was due to volatiles from the coal and not hydrogen. It is believed that the lower value is the truer one in light of the material balance calculations and lower H_2O vapor pressure at 250°C.

The maximum chemical reaction rate occurs at the coal feed point. When it is calculated using the larger of the k' values the result is 1.28 x 10-3 atm/s. Thus the maximum value of k' (assuming no mass-transfer resistance) is 1.28 x 10^{-3}/s.

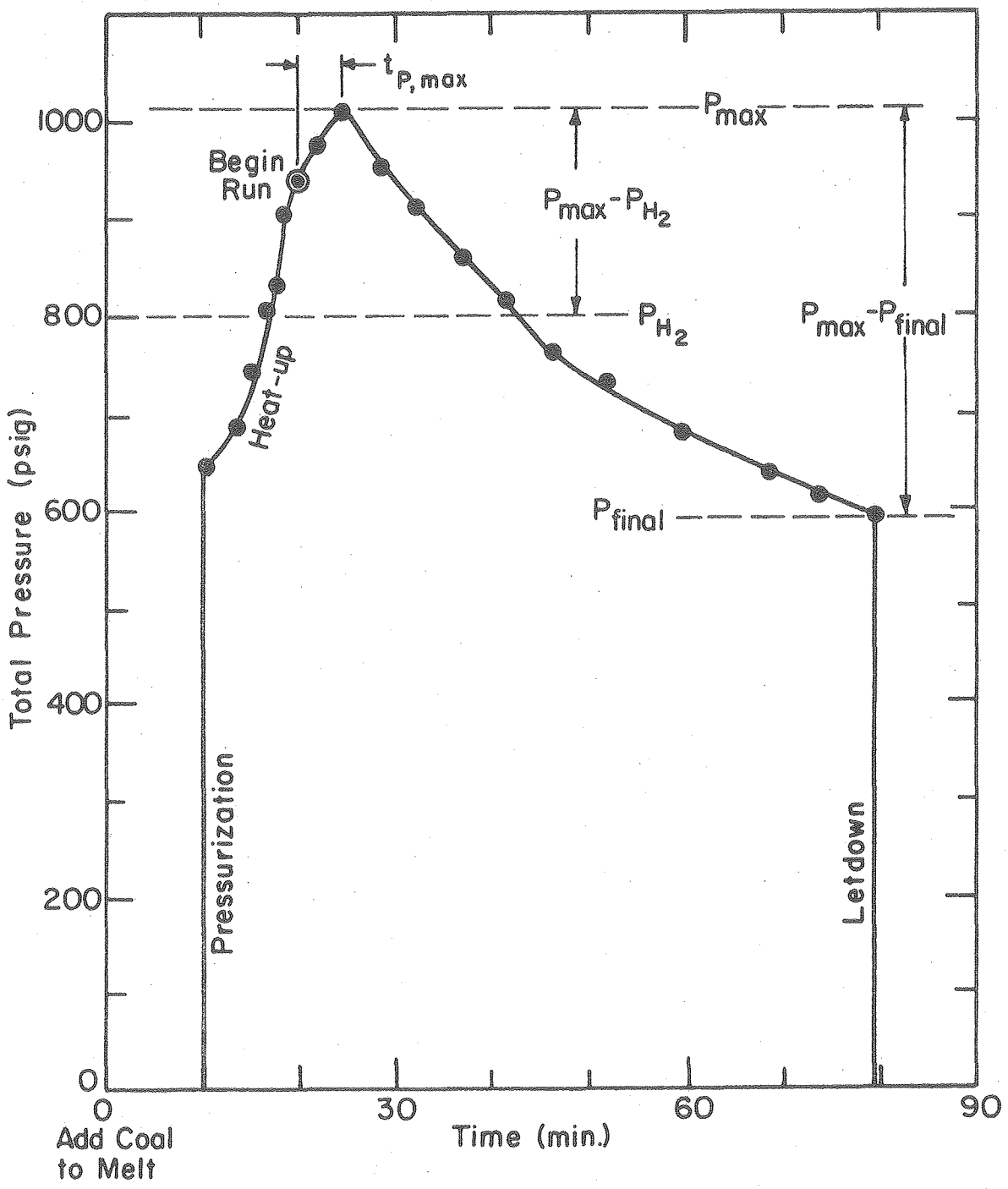

Figure VI-E1. Pressure-time data from Shinn (S9) run no. 72.

In the actual liquefaction reactor, the hydrogen pressure is constant and the rate expression becomes pseudo first order. When this expression is integrated, with the lower k' from Shinn's data and the molar ratio of carbon hydrogen in the feed is changed from 10.1 to 20.3 (33 wt% coal in the liquefaction reaction) the residence time becomes 25 minutes due to the constant hydrogen pressure and hence higher rate. This residence time is based on 250^{o}C and 600 psi hydrogen. If the process improvements discussed earlier are adopted, then the combined effects of higher temperature (275^{o}C in the top two sections and 325^{o}C in the bottom three) and gas scrubbing for water removal (to keep the catalytic activity of the melt as high as possible) should decrease this residence time to 15 minutes.

Appendix F

Hydrogen Requirement for the Coal Slurry Reactor

Calculations are shown here for the molar carbon throughput, minimum and 60% excess hydrogen, and maximum superficial gas velocity for 1 ft^3/min coal slurry flow in a reactor of 1 ft^2 cross-section.

Carbon

$$\frac{Ft^3}{Min}\ \text{Slurry} \times 124.7\ \frac{lb}{FT3} \times 0.3\ \frac{lb\ Coal}{lb\ Slurry} \times 0.63\ \frac{lb\ Carbon}{lb\ Coal}$$

$$\times\ \frac{lbmole\ Carbon}{12lb\ Carbon} = 1.96\ \frac{lbmole}{min}\ \text{Carbon}$$

Hydrogen

$$1.96\ \frac{lbmole}{min}\ \text{Carbon} \times \frac{lbmole\ Hydrogen}{4\ lbmole\ Carbon} \times 1.6 = 0.78\ \frac{lbmole}{min}$$

At 600 psi and 275^{o}C the maximum superficial gas velocity in any one section is obtained from adding hydrogen sparged to the left over from the previous section and

$$Ug\ max = \left[\frac{0.78}{1.6}\ (0.3) + 0.3\right] \frac{lbmoles}{min} \times 0.730\ \frac{ft^3\text{-}atm}{lbmole\text{-}^{o}R}$$

$$\times\ \frac{987^{o}R}{40.8\ atm} \times \frac{1}{ft^2} \times .3048 = 0.95\ \frac{meters}{min}$$

Appendix G

Gas-Liquid Mass Transfer from n-Propanol

The model liquids were purposely augmented with n-propanol in order to determine the mass transfer coefficients. The mass transfer data were reduced by using well known theory (S7). In terms of an overall driving force, for a nitrogen/n-propanol bubble rising in the column, the vapor phase concentration and mass transfer rates are

$$V_b \frac{dNp}{dz} - K_{og}\, a\, P(Y^*-Y) = 0 \qquad (1)$$

where

$$Np = \frac{PV_b}{RT} Yp \qquad (2)$$

and

$$Kog = \left[\frac{1}{Kg} + \frac{jP}{\bar{\rho} K_l}\right]^{-1} \qquad (3)$$

In terms of a bubble of equivalent spherical diameter, V_b/a becomes equal to $d_b/6$, and Equation 1 rearranges to

$$L = \int_0^L dz = \frac{d_b\, V_b}{K_{og}\, 6\, RT} \int_{Y_p=0}^{Y_p@L} \frac{dYp}{Y^*-Yp} \qquad (4)$$

The term before the integral represents the <u>height</u> of an overall gas-phase mass-transfer unit H_{og}, while the term under the integral is the <u>number</u> of overall gas-phase mass transfer units N_{og}. A plot of L vs. N_{og} yields a line whose slope is the average value of H_{og}.

Terms to account for the influence of the rate of mass transfer for water on that for n-propanol, or vice versa, were found not to be needed.

The molar gas phase concentrations, Y_p ad Y_p* were reduced from the raw chromatographic data as area fractions and the molar responds factors suggested by McNair (M3). The equilibrium mole fractions for water in n-propanol, Y_p*, were determined on two occasions in the 8 ft. high by 2 inches diameter columns each using three separate sample injections. The average of these injections are shown in Table IV G1. When these mole fractions are compared at the same temperature by making a vapor-pressure correction and assuming Raoult's Law, they agree to within 3.2% for water and 2.6% for n-propanol. Experimental proof that these data were the true equilibrium-vapor mole fractions was provided by changing the liquid height in the equilibrium column and finding that it had no effect on the resulting Y_p*'s.

Table VI G2 lists the mole fractions of n-propanol and water found in the model reactor as a function of height. When the vapor pressure correction is employed the overall number of gas-phase mass-transfer units can be calculated from

$$N_{og} = \int_{Y_p=0}^{Y_p@L} \frac{dY_p}{Y_p - Y_p^*} \qquad (5)$$

using a trapezoidal approximation method.

A plot of height vs. N_{og} is shown in Figure VI G1. The water peaks in the chromatograms were subject to tailing, and hence cannot be exactly correct.

The bubble size emanating from the 3/8" orifice under the same low gas flowrate, and liquid physical properties can be obtained from the photographic data of Quigley (Q1) et al. to be 2.91 cm. The rise velocity of bubbles with Reynolds numbers greater than 1 was found to be 38 cm/s from Mendelsohns' correlation (M4). With this information K_{og} from Figure VI-G1 was found to be 3.96×10^{-5} gmole/cm^2-s-atm. A gas-phase mass-transfer coefficient k_g calculated from the data of Geddes (G1) was found to be low enough to be considered, 1.21×10^{-4} gmols/cm^2-s-atm. From Equation 3 k_l was found to be 5.74×10^{-4} cm and $k_l a$ becomes 1.2×10^{-3} s^{-1}. If k_l were calculated according to the penetration theory, using the diffusivity of n-propanol in water with a correction for viscosity, the result would be 28×10^{-4} cm/s. Thus the measured result is 20% of that predicted by theory.

Errors in using other people's data on dissimilar systems could account for some of the discrepancy and there probably were errors introduced by mixing in the gas collection cone. However, it is believed that the temperature correction was so large that the calculation of N_{og} vs. ht resulted in a straight line that had little to do with the mass transfer taking place and that the k_l obtained is completely erroneous. It is believed that the results obtained in this mass transfer apparatus were in equilibrium with its surrounding liquid due the low value of the Henry's Law constant which is in the numerator of the resistance term for gas-liquid mass transfer.

Table VI-G1

Equilibrium Mole Fractions of Water and n-Propanol

Above 84cp Model Liquid

Temperature C	Mole Fraction	Vapor Pressure Torr
Water		
25	0.01864	23.8
29.5	0.02505	30.9
n-Propanol		
25	0.00929	19.7
29.5	0.01277	26.4

Table IV-G2

Mole Fraction, N_{og}, for Water and n-Propanol vs. Height for 3/8 Inch Orifice and Gas Flowrate of 0.078 ft^3/min.

Run No.	Temp. ^oC	Ht. cm.	Mole Fraction H_2O		Mole Fraction n-Propanol	
1	27	14	0.01629		0.00752	
	26	29	0.01756		0.00869	
2	23	14	0.01365		0.00583	
	24	22.5	0.01705		0.00674	
	23	29	0.01700		0.00717	
	Adjusted From Temperature to 25^oC					
				N_{og} H_2O		N_{og} n-Propanol
1	25	14	0.01448	1.4356	0.00660	1.1899
	25	29	0.01655	2.0458	0.00813	1.9755
2	25	14	0.01539	1.6272	0.00633	1.1125
	25	22.5	0.01801	2.8844	0.00720	1.4380
	25	29	0.01917		0.00818	2.0150

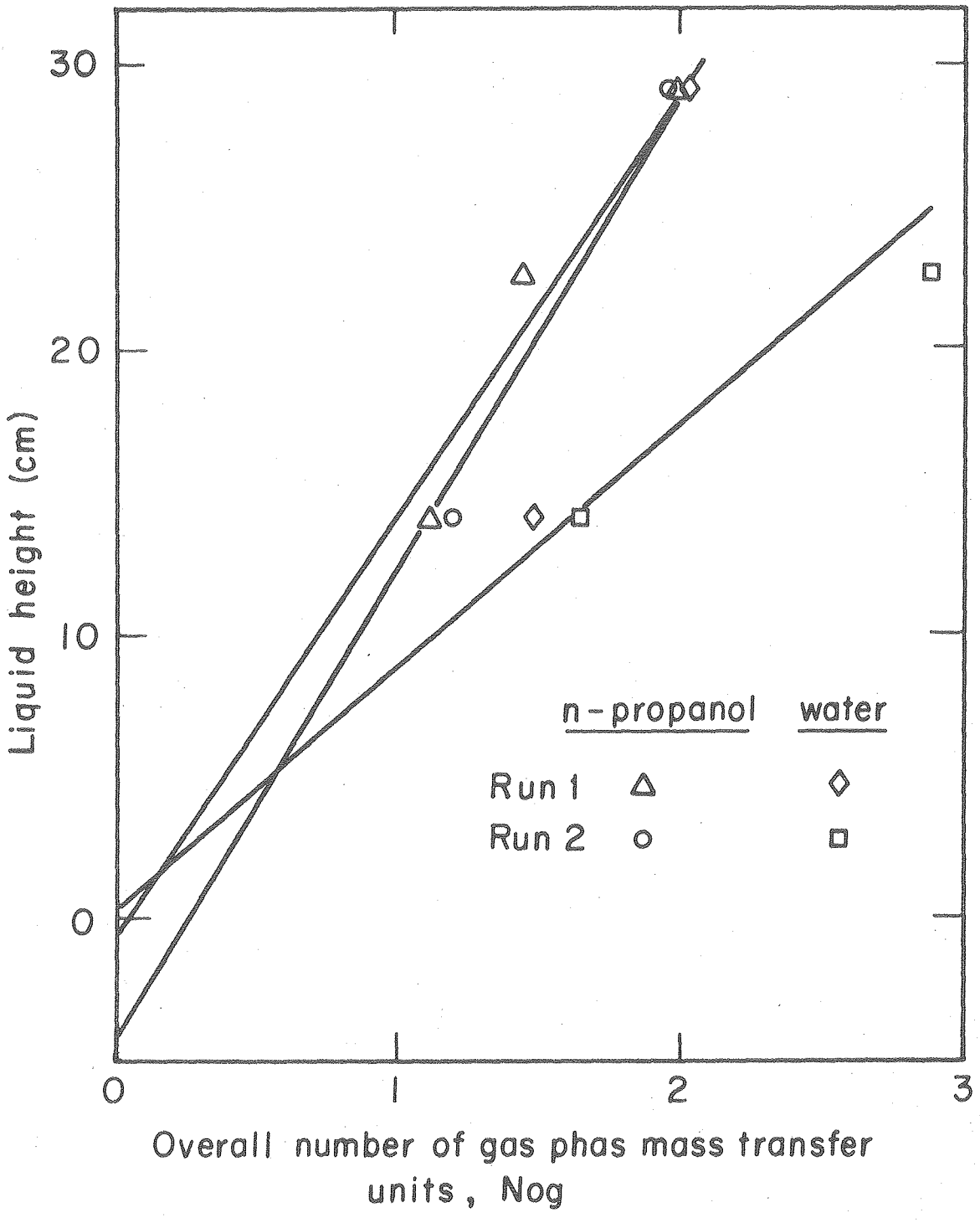

Figure VI-G1. Liquid height L_1 vs. N_{og} for n-propanol.

Notation

a	bubble interfacial area per unit volume of liquid (or slurry for 3 phase systems, cm^2/cm^3
B	constant for empirical viscosity correlating, gm/cm-s
a^p	particle interfacial area per unit volume of slurry, cm^2/
C_g	gas phase concentration, $gmole/cm^3$
C_{lg}	gas phase concentration at gas-liquid interface, $gmole/cm^3$
C_l	liquid phase concentration, $gmole/cm^3$
C_g^*	imaginary liquid phase concentration that would be in equilibrium with the gas, $gmole/cm^3$
C^o	helium concentration in gas at 1 atm partial pressure, $gmole/cm^3$
C_n	coal feed rate from stage n, lbmole/min
C_r	helium concentration at the recorder, $gmole/cm^3$
d_b	bubble diameter, cm
d_p	particle diameter, cm
D_c	column diameter, cm
D	diffusivity, cm^2/s
ΔE	activation energy for viscosity, kcal/gmole
F_n	average hydrogen molar flowrate, lbmole/min
f	fractional conversion of coal, dimensionless
G_n	water generated by chemical reaction in stage n, $\frac{\text{lbmole}}{\text{min}}$
g	gravitational acceleration, 980 cm/s^2
h_n	hydrogen entering stage n from nth stage, lbmole/min
H	Henry's Law constant, concentration ratio of dissolved gas in equilibrium between the gas and liquid phases, dimensionless

H' Henry's Law constant, atm/mole-fraction liquid

H_{og} height of an overall gas phase mass transfer unit, cm.

H_n hydrogen sparged to stage n of liquefaction reactor, lbmole/min

I internals volume, cm^3

j equilibrium line slope, dimensionless

k' second order coal conversion rate constant, $\frac{cm^3}{gmole\text{-}min}$ or $(atm\text{-}min)^{-1}$

k_g gas side mass transfer coefficient $\frac{gmole}{cm^2\text{-}s\text{-}atm}$ and

k_l liquid side mass transfer coefficient cm/s

K_{og} overall gas phase mass transfer coefficient $gmole/cm^2\text{-}s\text{-}atm$

K_o global rate coefficient for hydrogen absorption, s^{-1}

k_r lst order chemical reaction rate constant, s^{-1}

k_s liquid solid mass transfer coefficient cm/s

k_s^* liquid solid mass transfer coefficient, calculated at particle terminal velocity, cm/s

L Liquid froth height, cm

L_o settled liquid froth height, cm

m weight fraction of solids, dimensionless

M $k_{la}(1\text{-}e^{-\alpha})/\alpha$, dimensionless

n no. of gmoles charged to bubble column at the start of an experiment

N_p no. gmoles of n-propanol in the gas phase

N_{Sc} Schmidt No. $\mu/\rho\ d_b$

N_{Re} Bubble Reynolds No. $\frac{d_b v_b \rho}{\mu}$

P_{H_2} hydrogen pressure in Shinn's autoclave, psi

P_n water partial pressure in stage n, psi

P_{tot} Total liquefaction reactor pressure, psi

P_r helium partial pressure at the recorder, atm

q volumetric gas flowrate cm^3/s

R gas constant 82 cm^3-atm/^oK-gmole

r atomic radius, angstroms

S column cross sectional area

t time, seconds

$\bar{t}$ dimensionless time

T Temperature, ^oC

U_g Superficial column gas velocity m/min

$\tilde{v}$ molar volume of dissolved gas, gmole/cm^3

V_t total gas volume passed through bubble column during an experiment, cm^3

V_b bubble volume, cm^3

V_d dead volume of gas above liquid in bubble column, cm^3

V_l liquid volume in column, cm^3

v_b bubble rise velocity, cm/s

v_p^* particle terminal velocity

W_w water weight fraction in $ZnCl_2$ melt in stage n from Holton, dimensionless

W_n water weight fraction in stage n, dimensionless

X_n water liquid molar flowrate from stage n, lbmole/min

Y_2' water stream sent to scrubber, lbmole/min

Y_n water gaseous molar flowrate to stage n, lbmole/min

Y_p mole fraction of n-propanol, dimensionless

Y_p^* equilibrium mole fraction of n-propanol, dimensionless

z vertical column height, cm

Section IV,

α defined by equation 9, dimensionless

δ liquid film thickness, cm

ε_g volume fraction of gas based on liquid or slurry, dimensionless

σ surface tension, dynes/cm

τ_d gas phase dead volume time constant, $U_g/q\ S$

$\bar{\rho}$ molal density of melt, gmole/gm

ρ density, gm/cm^3; density difference between gas and liquid

η effectiveness factor, dimensionless

μ viscosity $\frac{gm}{cm\text{-}s}$; $_c$ continuous phase

ν_l kinematic viscosity of liquid, cm/s

References

A1 Akita, K., Yoshida, F., "Gas Holdup and Volumetric Mass Transfer Coefficient in Bubble Columns," Ind. Eng. Chem. Proc. Des. Dev.; V12, No. 1, 76, 1973.

A2 Akita, K., Yoshida, F., "Bubble Size, Interfacial Area, Liquid Phase Mass Transfer Coefficient in Bubble Column," Ind. Eng. Chem. Proc. Des. Dev., V13, No. 1, 84 1974.

A3 Anderson, R. P., "The SRC II Process," ACS Preprints, 22, No. 6, 132, 1977.

B1 Bhavaraju, S. M., Russell, T. W. F., Blanch, H. W., "The Design of Gas Sparged Devices for Viscous Liquid System," AIChE J., V24, No. 3, 454, May 1978.

B2 Brelvi, W. S., O'Connell, J. P., "Prediction of Unsymmetric Convention Liquid-Phase Activity Coefficients of Hydrogen and Methane," AIChE J., V21, No. 1, 157, January 1975.

B33 Brian, P.L.T., Hales, H. R., "Effects of Transpiration and Changing Diameter on Heat and Mass Transfer to Spheres," AIChE J., V15, No. 3, 419, May 1969.

C1 Calderbank, P. H., Moo-Young, M.B., "The Continuous Phase Heat and Mass Transfer Properties of Dispersions," Chem. Eng. Sci., V16, 39, 1961.

C2 Cochran, N. P., "Oil and Gas from Coal," Scientific American V234, No. 5, 24, May 1976.

C3 Cova, D. R., "Catalyst Suspension in Gas Agitated Tubular Reactors", Ind. Eng. Chem. Proc. Des. and Dev., 5, No. 1, 23, January 1966.

D1 Darton, R. C., Harrison, D. R., "Gas and Liquid Hold-up in Three Phase Fluidization," Chem. Eng. Sci., V30, 581, 1975.

E1 "Exxon Donor Solvent Coal Liquefaction Process Development," Phases IIIB/IV, FE-2893-17, 4, September 1978.

E2 Ellis, J. E., Jones, E. L., Two Phase Flow Symposium, Exeter, England, June 1965.

G1 Geddes, R.L., Trans. Am. Inst. Chem. Engrs., V42, 79, 1946.

G2 Goto, S., Smith, J. M. "Performance of Slurry and Trickle Bed Application to SO_2 Removal," AIChE J., V24, No. 2, 286, March 1978.

G3 Gouse, S. W., Jr., "An Index to the Two Phase Gas Liquid Flow Literature," M.I.T. Press, Cambridge, Mass., 1966.

G4 Govindaro, V. M. H., "On the Dynamics of Bubble Column Slurry Reactors," Chem. Eng. J., V9, 229, 1975.

G5 Gubbins, K. E., Kamlesh, B. K., Walker, R. D., "Diffusion of Gases in Electrolytic Solutions," AIChE J., V12, No. 3, 548, May 1966.

G6 Guin, J. A., Tarrer, A. R., Pitts, W. S., Prather, J. W., "Kinetics and Solubility of Hydrogen in Coal Liquefaction Reactions," ACS Preprints, V21, No. 5, 170, September 1976.

H1 "H-Coal Integrated Pilot Plant" EPRI #AF681, V2, 2-1, March 1978.

H2 Hershkowitz, F., private communication.

H3 Higbie, R., Trans. AIChE, V31, 365, 1935.

H4 Hiss, T. G., Cussler, E. L., "Diffusion in High Viscosity Liquids," AIChE J., V19, No. 4, 698, July 1973.

H5 Holton, R., M.S. Thesis, University of California at Berkeley, December 1977.

H6 Hughmark, G. A., "Holdup and Mass Transfer in Bubble Columns," Ind. Eng. Chem. Proc. Des. Dev., 219, V6, No. 2, April 1967.

H7 Hughmark, G. A., "Mass and Heat Transfer from Rigid Spheres," AIChE J., V13, No. 6, 1219, November 1967.

J1 Javdani, K., Schwalbe, S., Fischer, J., "Multiphase Flow of Gas-Liquid and Gas-Coal Slurry Mixtures in Vertical Tubes," ANL-76-116, January 1977.

J2 Joosten, G. E. H., Schilder, J. G. M., Janssen, J. J., "The Influence of Suspended Solid Material on the Gas-Liquid Mass Transfer in Stirred Gas-Liquid Contactors," Chem. Eng. Sci., V32, 563, 1977.

J3 Juvekar, J. M., Sharma, M. M., "Absorption of CO_2 in a Suspension of Lime," Chem. Eng. Sci., V28, 825, 1973.

K1 Kato, Y., "Gas-Liquid Contact in a Gas-Liquid-Solid Fluidized Bed," Kagakū, Kogukū, Vol. 1, No. 1, 3, 1963.

K2 Kim, S. D., Baker, J. G. C., Bergougnov, M. S., "Bubble Characteristics in Three Phase Fluidized Beds," Chem. Eng. Sci, 1299, Vol. 32, 1977.

K3 Ibid., "Phase Holdup Characteristics of Three Phase Fluidized Beds," Can. J. Chem. Eng., V3, 134, April 1975.

K4 Ibid., "Holdup and Axial Mixing Characteristics of Two and Three Phase Fluidized Beds," Can. J. Chem. Eng., V50, 695, Dec. 1972.

R3 Razumov, I. M., Manshilin, V. V., Nemets, L. L., "The Structure of Three Phase Fluidized Beds," International Chemical Engineering V13, No. 1, 57, January 1973.

R4 Rigby, G. R., Van Blockland, G. P., Park, W. H., Capes, C. E., "Properties of Bubbles in Three Phase Fluidized Beds as Measured by an Electrosensitivity Probe," Chem. Eng. Sci., V25, 1729, 1970.

S1 Sada, E., Kumazawa, H., Butt, M. A. "Single Gas Absorption with Reaction in a Slurry Containing Fine Particles," Chem. Eng. Sci., V32, 1165, 1977.

S2 Satterfield, C. N., "Mass Transfer in Heterogeneous Catalysis," MIT Press, Cambridge Mass, 107, 1970.

S3 Schaftlein, R. W., Russell, T. W., "Two Phase Reactor Design," Ind. Eng. Chem., V60, No. 5, 13, May 1968.

S4 Shah, Y. T., "Gas-Liquid-Solid Reactor Design," McGraw Hill, Inc., 1979.

S5 Sharma, M. M., Mashelkar, R. A., Paper presented at the Tripartite Chem. Eng. Conf., Symposium on Mass Transfer with Chemical Reaction, Montreal, September 1968.

S6 Sherwood, T. K., Farkas, E. J., "Studies of the Slurry Reactor," Chem. Eng. Sci., V21, 573, 1966.

S7 Sherwood, T. K., Pigford, R. L., Wilke, C. R., "Mass Transfer," McGraw Hill, 1975.

S8 Shinn, J. H., PhD Thesis, the University of California at Berkeley, 1979.

K5 Komiyama, H., Smith, J. M., "Sulfur Dioxide Oxidation in Slurries of Activated Carbon," AIChE J., Vol 21, No. 4, 664, July 1975.

M1 Mushelkar, R. A., "Bubble Columns," British Chem. Eng., Vol. 15, No. 10, 1297, Oct. 1979.

M2 Mushelkar, R. A., Sharma, M. M., "Mass Transfer in Bubble and Packed Columns," Trans. Instn. Chem. Engrs., V48, T162, 1970.

M3 McNair, H. M., Bonelli, E. J., "Basic Gas Chromatography," Consolidated Printers, Berkeley, CA, 153-157, March 1969.

M4 Mendelson, H. D., "The Prediction of Bubble Terminal Velocity from Wave Theory," AIChE J., V13, 250, 1967.

M5 Misic, D. M., Smith, J. M., "Adsorption of Benzene in Carbon Slurries," Ind. Eng. Chem., V10, No. 3, 380, 1971.

N1 Niyama, H., Smith, J. M., "Adsorption of Nitric Oxide in Aqueous Slurries of Activated Carbon. Transport Rates by Moment Analysis of Dynamic Data," AIChE J., V22, No. 6, 961, 1976.

P1 Perry, R. H., Chilton, C. H., Kirkpatrik, S. D., "Chemical Engineers Handbook," McGraw Hill, 4th Ed., 14-5, 1963.

Q1 Quigley, C. J., Johnson, A. I., Harris, B. L., "Size and Mass Transfer Studies of Gas Bubbles," Chem. Eng. Progr. Symp. Series, V51, No. 16, 31, 1965.

R1 Ramachandran, P. A., Sharma, M. M., "Absorption with Fast Reaction in a Slurry Containing Sparingly Soluble Fine Particles," Chem. Eng. Sci., V24, 1681, 1969.

R2 Ramachandran, P. A., Smith, J. M., "Dynamics of a Three Phase Slurry Reactor," Chem. Eng. Sci., V32, 1277, 1977.

S9 Shinn, John H., Hershkowitz, F., Holten, R., Vermuelen, T., Grens, E. A., "Coal Liquefaction in Inorganic-Organic Liquid Mixtures, AIChE Symposium on Reaction Engineering in Coal Processes, Miami, November 1978.

S10 Simmick, J. J., Lawson, C. C., Lin, H. M., Chao, K. C., "Vapor Liquid Equilibrium of Hydrogen/Tetralin Systems at Elevated Temperatures and Pressures," AIChE J., V23, No. 4, 470, July 1977.

S11 Struck, R. T., Clark, W. E., Dudt, P. J., Rosenhoover, W. A., Zielke, C. W., Gorin, E., "Kinetics of Hydrocracking Coal Extract with Molten $ZnCl_2$ Catalysts," Ind. Eng. Chem. Proc. Des. Dev., V8, 551, October 1969.

T1 Towell, G. D., Strand, C. P., Ackerman, G. H., "Mixing and Mass Transfer in Large Diameter Bubble Columns," AIChE Symposium Series, No. 10, 1965 (London: Instn. Chem. Engrs.).

T2 "Turbogrid Distillation Trays," Chem. Eng. Progress, V50, No. 2, 57, Engineering Staff of Shell Development Co., February 1954.

U1 Uchida, S., Wen, C. Y., "Rate of Gas Absorption into a Slurry Accompanied by Instantaneous Reaction," Chem. Eng. Sci., V32, 1277, 1977.

U2 Ibid., "Gas Absorption with Fast Reaction Into a Slurry: Case of Fast Absorption Rate Compared with Solid Dissolution Rate," Chem. Eng. Sci., V32, 447, 1977.

V1 Vermeer, D., Private Communication.

W1 Watson, G. R., Evans, R. B., Grimes, W. R., Smith, N. V., "Solubility of Noble Gases in Molten Fluorides," J. Chem. Eng. Data, V7, No. 2, April 1962.

W2 Wen, C. Y., "Fossil Energy," Quarterly Report, July to September 1976.

W3 Ibid., "Fossil Energy," Quarterly Report, October to December 1976.

Y1 Yoshida, F., Akita, K., "Performance of Gas Bubble Columns: Volumetric Liquid Phase Mass Transfer Coefficient and Gas Holdup," AIChE J., V11, No. 1, 9, 1965.

Y2 Yoshitome, H., "Average Ascending Velocity of Air Bubbles in Water from Perforated Plates," Kagaku, Kagaku, V1, No., 20, 1963.

TECHNICAL INFORMATION DEPARTMENT
LAWRENCE BERKELEY LABORATORY
UNIVERSITY OF CALIFORNIA
BERKELEY, CALIFORNIA 94720